Neisseria species as pathobionts in bronchiectasis

Li, Liang; Mac Aogáin, Micheál; Xu, Tengfei; Jaggi, Tavleen Kaur; Chan, Louisa L.Y.; Qu, Jing

Published in:
Cell Host & Microbe

DOI:
10.1016/j.chom.2022.08.005

Publication date:
2022

Clinical and Translational Report

Cell Host & Microbe

Neisseria species as pathobionts in bronchiectasis

Graphical abstract

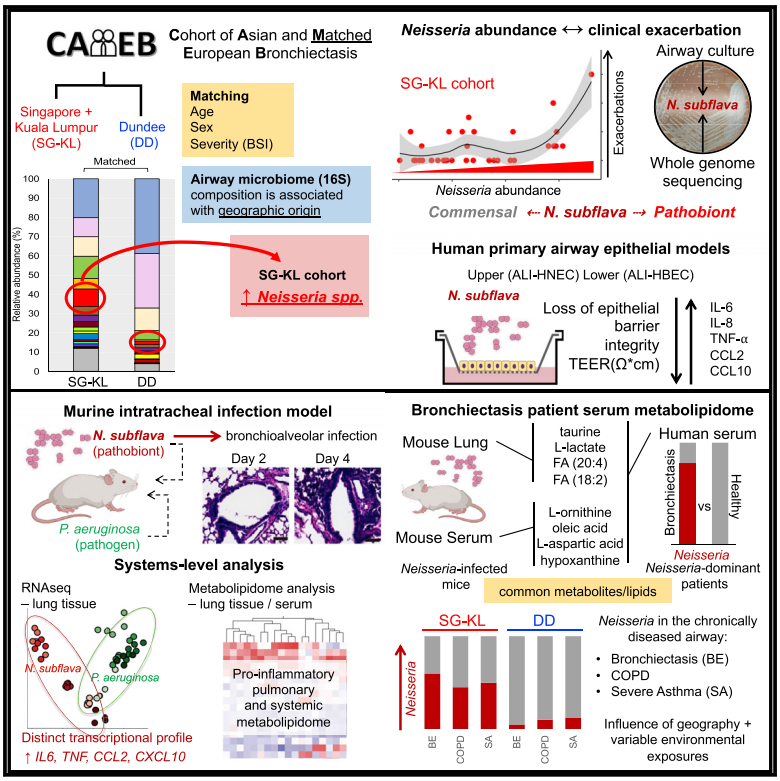

Highlights

- Some bronchiectasis patients exhibit increased airway abundance of *Neisseria* spp.
- The culturable species *N. subflava* weakens barrier integrity and induces inflammation
- *N. subflava* elicits distinct transcriptomic/metabolipidomic signatures in the mouse lung
- *Neisseria*-associated pathogenic signatures are observed in bronchiectasis patients

Authors

Liang Li, Micheál Mac Aogáin, Tengfei Xu, ..., Mingliang Fang, James D. Chalmers, Sanjay H. Chotirmall

Correspondence

schotirmall@ntu.edu.sg

In brief

Bronchiectasis exhibits geographically variable airway microbiomes, including an increased abundance of *Neisseriaceae,* which is linked to exacerbations. Systems-level analysis of clinical *N. subflava* identified distinct transcriptomic and metabolipidomic profiles in a murine model of airway exposure. These signatures concurred with those observed in human *Neisseria*-dominant patients with bronchiectasis, supporting a "pathobiont" role for *Neisseria*.

Li et al., 2022, Cell Host & Microbe *30*, 1311–1327
September 14, 2022
https://doi.org/10.1016/j.chom.2022.08.005

CellPress

Cell Host & Microbe

CellPress
OPEN ACCESS

Clinical and Translational Report

Neisseria species as pathobionts in bronchiectasis

Liang Li,[1,2,22] Micheál Mac Aogáin,[3,4,5,22] Tengfei Xu,[6,7,22] Tavleen Kaur Jaggi,[3] Louisa L.Y. Chan,[3] Jing Qu,[2] Lan Wei,[2] Shumin Liao,[2] Hong Sheng Cheng,[3] Holly R. Keir,[8] Alison J. Dicker,[8] Kai Sen Tan,[9] Wang De Yun,[9] Mariko Siyue Koh,[10] Thun How Ong,[10] Albert Yick Hou Lim,[11] John A. Abisheganaden,[3,11] Teck Boon Low,[12] Tidi Maharani Hassan,[13] Xiang Long,[14] Peter A.B. Wark,[15,16] Brian Oliver,[17,18] Daniela I. Drautz-Moses,[19] Stephan C. Schuster,[19] Nguan Soon Tan,[3,20] Mingliang Fang,[6,21] James D. Chalmers,[8] and Sanjay H. Chotirmall[3,11,23,*]

[1]Department of Pharmacology, School of Medicine, Southern University of Science and Technology, Shenzhen, China
[2]Shenzhen Institutes of Advanced Technology, Chinese Academy of Sciences, Shenzhen, China
[3]Lee Kong Chian School of Medicine, Nanyang Technological University, Singapore, Singapore
[4]Biochemical Genetics Laboratory, Department of Biochemistry, St. James's Hospital, Dublin, Ireland
[5]Clinical Biochemistry Unit, School of Medicine, Trinity College Dublin, Dublin, Ireland
[6]School of Civil and Environmental Engineering, Nanyang Technological University, Singapore, Singapore
[7]College of Pharmaceutical Sciences, Zhejiang University, Hangzhou 310058, PRC
[8]University of Dundee, Ninewells Hospital, Medical School, Dundee, Scotland
[9]Department of Otolaryngology, Infectious Disease Translational Research Programme, Yong Loo Lin School of Medicine, National University of Singapore, Singapore, Singapore
[10]Department of Respiratory and Critical Care Medicine, Singapore General Hospital, Singapore, Singapore
[11]Department of Respiratory and Critical Care Medicine, Tan Tock Seng Hospital, Singapore, Singapore
[12]Department of Respiratory and Critical Care Medicine, Changi General Hospital, Singapore, Singapore
[13]Universiti Kebangsaan Malaysia, Kuala Lumpur, Malaysia
[14]Department of Respiratory Medicine and Critical Care, Peking University Shenzhen Hospital, Shenzhen, China
[15]Priority Research Centre for Healthy Lungs, Hunter Medical Research Institute, School of Medicine and Public Health, University of Newcastle, Newcastle, NSW, Australia
[16]Department of Respiratory and Sleep Medicine, John Hunter Hospital, New Lambton Heights, NSW, Australia
[17]Woolcock Institute of Medical Research, University of Sydney, Sydney, NSW, Australia
[18]School of Life Sciences, University of Technology Sydney, Sydney, NSW, Australia
[19]Singapore Centre for Environmental Life Sciences Engineering (SCELSE), Nanyang Technological University, Singapore, Singapore
[20]School of Biological Sciences, Nanyang Technological University, Singapore, Singapore
[21]Department of Environmental Science and Engineering, Fudan University, Shanghai 200433, China
[22]These authors contributed equally
[23]Lead contact
*Correspondence: schotirmall@ntu.edu.sg
https://doi.org/10.1016/j.chom.2022.08.005

SUMMARY

Neisseria species are frequently identified in the bronchiectasis microbiome, but they are regarded as respiratory commensals. Using a combination of human cohorts, next-generation sequencing, systems biology, and animal models, we show that bronchiectasis bacteriomes defined by the presence of *Neisseria* spp. associate with poor clinical outcomes, including exacerbations. *Neisseria subflava* cultivated from bronchiectasis patients promotes the loss of epithelial integrity and inflammation in primary epithelial cells. *In vivo* animal models of *Neisseria subflava* infection and metabolipidome analysis highlight immunoinflammatory functional gene clusters and provide evidence for pulmonary inflammation. The murine metabolipidomic data were validated with human *Neisseria*-dominant bronchiectasis samples and compared with disease in which *Pseudomonas*-, an established bronchiectasis pathogen, is dominant. Metagenomic surveillance of *Neisseria* across various respiratory disorders reveals broader importance, and the assessment of the home environment in bronchiectasis implies potential environmental sources of exposure. Thus, we identify *Neisseria* species as pathobionts in bronchiectasis, allowing for improved risk stratification in this high-risk group.

INTRODUCTION

The study of microbes in chronic respiratory disease is evolving. Departing from traditional single pathogen-centric models to more holistic and integrative approaches will facilitate an appreciation of the airway microbiome composition and its associated host response (Budden et al., 2019; O'Dwyer et al., 2016).

Microbial networks, composed of pathogenic and commensal "pathobiont" constituents, and understanding the microbiome better defines airway ecology and the associated clinical

endophenotypes of respiratory disease (Gao et al., 2018; Layeghifard et al., 2019; Mac Aogáin et al., 2021). Recent work suggests that commensal airway bacteria play dynamic roles in shaping the host immune response, including the maintenance of mucosal homeostasis where micro-aspiration of upper airway taxa engenders robust immune tone and protection from pathogenic microbes (Wu et al., 2021). These observations align with human studies that define subclinical microbiome-related clusters that exhibit distinct metabolic profiles, enhanced expression of inflammatory cytokines, and elevated Th17 lymphocytes (Segal et al., 2016). As such, the microbiome potentially exerts influence across a spectrum of clinical states and disease endophenotypes, from daily homeostatic interaction with host immunity that dictates subclinical immunophenotypes to a more extreme dysregulated immune-inflammatory milieu observed in the chronically diseased airway (Richardson et al., 2019).

Bronchiectasis, a disease characterized by permanent, progressive, and irreversible dilatation of the airways, is increasing in prevalence globally (Chalmers et al., 2018; Dhar et al., 2019). Renewed focus on its molecular underpinning has led to improved understanding of this complex and heterogeneous condition, including the association of microbiome composition with clinical phenotype (Chalmers and Chotirmall, 2018; Flume et al., 2018; Mac Aogáin et al., 2021; Metersky and Chalmers, 2019). Recurrent cycles of infection and inflammation characterize its pathogenesis and result in structural abnormalities; however, the inherent clinical heterogeneity is exemplified by failed clinical trials due to marked differences between patients and their response to therapy (Chotirmall, 2018; Chotirmall and Chalmers, 2018; Flume et al., 2018). Chronic infection is a hallmark of bronchiectasis, and infection represents a cause and consequence of disease; however, the identification of potential culprit pathogens exhibits considerable geographic variation. In 1 of 3 patients, sputum cultures are negative, despite a detectable inflammatory response and clinical phenotype suggestive of chronic infection (Dickson et al., 2013; Fuschillo et al., 2008; Richardson et al., 2019). Recent work highlights the importance of geographic variation to microbiomes in bronchiectasis, including a failure to replicate key findings from partner clinical trials such as RESPIRE (Aksamit et al., 2018; Chotirmall and Chalmers, 2018; Chotirmall et al., 2017; De Soyza et al., 2018). Taken together, these data underscore the complex and heterogeneous microbial consortia associated with bronchiectasis; however, they provide potential scope for their use in improving patient stratification (Mac Aogáin et al., 2021; Rogers et al., 2014b). Although microbiomes associate with clinical phenotypes in bronchiectasis, studies accounting for geographic variation and which advance testable hypotheses or provide mechanisms for such observations remain limited. Furthermore, "classical" bronchiectasis pathogens, including *S. pneumoniae*, *H. influenzae*, and gram-negative organisms such as *Pseudomonas aeruginosa*, all identified for their ability to cause invasive pneumonia, do not account for the possibility that upper airway commensals, which cause local inflammation but not necessarily bloodstream infection, may have pathogenic roles.

Here, we leverage on the cohort of Asian and matched European bronchiectasis (CAMEB) and employ a bedside-to-bench approach using a combination of next-generation sequencing and systems biology to identify and characterize *Neisseria* spp. as pathobionts in bronchiectasis. We demonstrate (in geographically matched individuals) that *Neisseria* spp. is associated with poorer clinical outcomes in bronchiectasis and that *Neisseria subflava* demonstrates immunopathologic potential in primary human cell and mouse infection models. The multiomics response to *Neisseria subflava* infection was characterized and integrated using transcriptomic, metabolomic, and lipidomic approaches, with validation in patients with bronchiectasis corroborating its "pathobiont" role. Finally, we demonstrate that *Neisseria* spp. can be identified in other respiratory diseases and indoor environments. Identifying *Neisseria* species as pathobionts in bronchiectasis allows improved patient risk stratification and potential intervention.

RESULTS

Bacteriomes demonstrate geographic variation characterized by *Neisseria* species

We performed 16S targeted amplicon sequencing of the airway microbiome in the CAMEB cohort which "matched" individuals of Asian (Singapore-Kuala Lumpur, Malaysia [SG-KL]) and European (Dundee, Scotland [DD]) origin by age, sex, and disease severity (n = 225; Table S1) (Mac Aogáin et al., 2018). This revealed geographic differences characterized by established bronchiectasis pathogens, including *Pseudomonas*, *Haemophilus*, *Streptococcus*, and *Moraxella* and included *Neisseria* spp., considered commensal, but represent the predominant discriminant bacterial taxa in Asians (Figures 1A–1F and S1; Rogers et al., 2014b). *Neisseria* spp. were overrepresented in Asians (Figures 1A–1D), corroborated by linear discriminate analysis (LDA) effect size (LEfSe) (Figures 1E and 1F). Having identified *Neisseria* spp. by a growth-independent methodology, we next evaluated n = 10 Asian airway specimens (with the highest relative abundance of *Neisseria* spp. by 16S sequencing) for the presence of *Neisseria* isolates. Growth-based assessment identified multiple specimens yielding significant growth of gray unpigmented colonies on chocolate agar, consistent with *Neisseria* morphology. Commercial biochemical and MALDI TOF bacterial identification assays were consistent with the identification of these isolates as members of the genus *Neisseria* (data not shown). This was further confirmed by whole-genome sequencing and phylogenetic analyses identifying isolates to the species level as *N. subflava* based on comparison of high-quality genome assemblies with publicly available reference genomes (Figure 1G). To prove this organism was present in the lower airway and not simply transiently detected due to aspiration from the upper respiratory tract, fluorescent *in situ* hybridization (FISH) probes specific for *N. subflava* were designed (see key resources table) and used to assess formalin-fixed-paraffin-embedded lung tissue biopsies obtained from control individuals (n = 12, lung cancer without bronchiectasis) and individuals with bronchiectasis and *Neisseria*-dominant 16S microbiome profiles (n = 9) (Table S2). FISH imaging confirmed *N. subflava* in the lower airways of individuals with bronchiectasis (Figure 1H). Sub-analysis of Asians exhibiting *Neisseria*-dominant profiles revealed a significant correlation between *Neisseria* abundance and exacerbation frequency independent of disease severity, lung function, or sputum bacterial 16S ribosomal RNA (rRNA) amplicon concentration and/or read counts (Figures 1I

CellPress
OPEN ACCESS

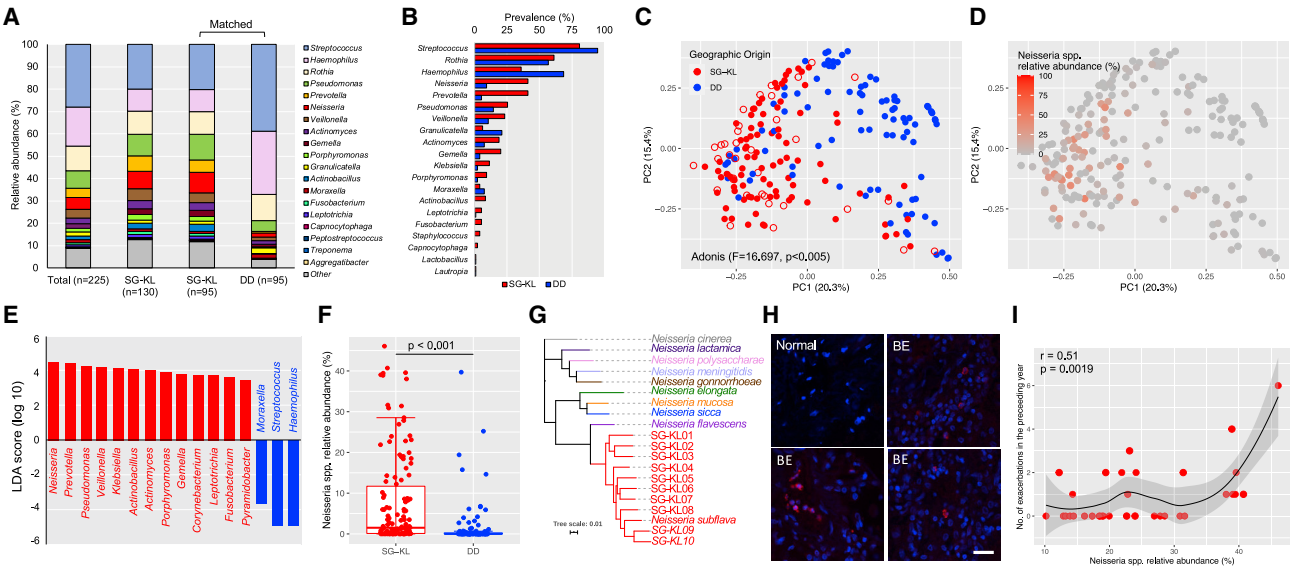

Figure 1. The airway microbiome in bronchiectasis demonstrates geographic variation characterized by *Neisseria* spp

(A) Matched 16S bacteriome profiles in Asians (Singapore and Kuala Lumpur, Malaysia [SG-KL]) and non-Asians (Dundee, Scotland [DD]). Stacked bar charts illustrating bacteriome profiles in the CAMEB cohort (n = 225), those in Asians (SG-KL, n = 130) and in a subset of n = 95 patients matched across jurisdictions based on age, sex, and bronchiectasis severity, based on bronchiectasis severity index (BSI).

(B) Prevalence of the top 20 bacterial genera present at >5% relative abundance in the SG-KL (Asians; red) and DD (non-Asians; blue) cohorts, respectively.

(C) Principal coordinate analysis (PCoA) demonstrating geographic variation in bacteriome profiles. Individual profiles are illustrated by red (SG-KL; n = 130) and blue (DD, n = 95) dot coloration, respectively, with filled circles indicating matched and open circles unmatched individuals (n = 95 in each group). The F-ratio and associated p value for adonis PERMANOVA analysis are indicated.

(D) Principal coordinate analysis (PCoA) highlighting an increased relative abundance of *Neisseria* spp. in the SG-KL group. PCoA plot coloration depth (red) indicates the relative abundance of *Neisseria* spp. based on percentage (%) of assigned reads.

(E and F) (E) Linear discriminate analysis (LDA) highlighting *Neisseria* spp. among the top discriminant taxa in the SG-KL cohort and (F) box plot illustrating a higher relative abundance of *Neisseria* spp. in the SG-KL cohort. The p value associated with Mann-Whitney U-test (SG-KL versus DD) is indicated. Box plots indicate the inter quartile range (IQR) with the bisecting lines representative of the median and whiskers representing 1.5 times the IQR.

(G) Culturable *Neisseria* isolates from the SG-KL cohort reveal *Neisseria subflava* as the predominant species. Phylogenetic core genome analysis using high-quality, PacBio-derived complete genome sequences of cultured *Neisseria* isolates (from this study) and publicly available *Neisseria* genome sequences. Tree scale indicates nucleotide substitutions per site, and tree nodes are colored by species classification of the associated reference genome; red coloration represents clinical isolates from the SG-KL cohort and their most closely related reference sequence: *N. subflava* (NJ9703).

(H) Fluorescent *in situ* hybridization (FISH) detection of *N. subflava* in lung tissue from non-diseased individuals (controls) (n = 12) and individuals with bronchiectasis (BE, n = 9). Only a single representative image for non-diseased (no detection) and three for bronchiectasis (with *N. subflava* detection) are illustrated. Probes are based on the *N. subflava* genome. DAPI staining (blue) indicates cell nuclei, and FISH detection (red) illustrates *N. subflava*. Scale bars, 20 μm.

(I) Increased exacerbation frequency correlates with increased relative abundance of airway *Neisseria* spp. (≥10% of relative bacteriome composition) in the SG-KL cohort (n = 34). Pearson's r and associated p value are indicated.

and S2). There was no observed effect of either antibiotics or inhaled corticosteroids on *Neisseria* abundance (Mann-Whitney U test, $p > 0.05$) or dominance (chi-squared, $p > 0.05$) in Asian patients. Taken together, these findings potentially implicate *Neisseria* spp. as airway pathobionts in bronchiectasis where it associates with increased exacerbations.

Airway *N. subflava* infection promotes loss of epithelial barrier integrity and induces inflammation

To assess the ability of the *Neisseria subflava* isolates to infect the human airway, we employed primary differentiated human nasopharyngeal epithelial cells (HNECs) and human bronchial epithelial cells (HBECs) at air-liquid interface (ALI), representative of the upper and lower airways, respectively. Primary airway epithelial cells were susceptible to infection and *N. subflava* rRNA was detectable as early as 2 h post infection (hpi). *N. subflava* was internalized by 24 hpi with intracellular bacterial load peaking at 72 hpi, as quantified by qRT-PCR of cell lysates (Figure 2A). Significant disruption of the epithelial cell-cell barrier was demonstrable through reduction in *trans*-epithelial electrical resistance (TEER) (Figures 2B and 2C). *Neisseria subflava* infection triggered airway inflammatory responses characterized by increased gene expression of interleukin (IL)-6, IL-8, CCL2, and CXCL10 (Figures 2D–2H).

Intratracheal administration of *N. subflava* induces bronchioalveolar infection and immunoinflammatory responses *in vivo*

Intratracheal delivery of clinical *N. subflava* isolates to C57BL/6 mice resulted in decreased body weight and clinical score indicative of successful infection (Figures 3A and 3B). For both *N. subflava* and the *P. aeruginosa* comparator group, mouse body weight dropped at day 2 post infection and increased thereafter (Figure 3A). *P. aeruginosa* infected mice show poorer outcomes at day 2, demonstrating a rapid evolution of infection when compared with *N. subflava* (Figure 3B). The bacterial load

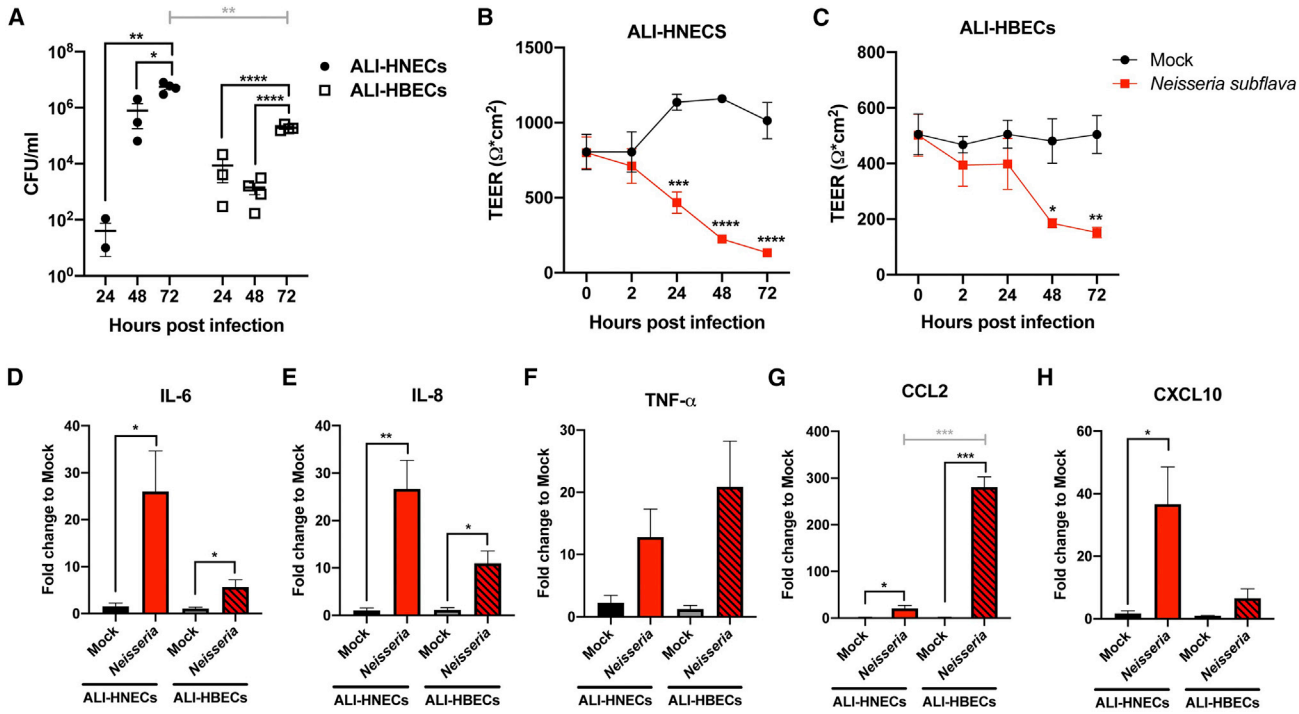

Figure 2. *N. subflava* infection of primary human epithelial cells at air-liquid interface reveals a loss of barrier integrity and enhanced inflammation

(A) Primary human ALI-HNECs and ALI-HBECs infected with *N. subflava* had internalized bacteria quantified by colony counts and expressed as CFU/mL at 24, 48, and 72 hpi.

(B and C) TEER measurements, evaluating epithelial barrier integrity, taken at 0, 2, 24, 48, and 72 hpi in mock or *N. subflava*-infected (B) ALI-HNECs and (C) ALI-HBECs.

(D–H) qRT-PCR analyses of cell lysates harvested at 24 hpi evaluating pro-inflammatory gene expression for the cytokines (D) IL-6, (E) IL-8, and (F) TNF-α and the chemokines (G) CCL2 and (H) CXCL10 following mock or *N. subflava* infection of ALI-HNECs (left) and ALI-HBECs (right). Fold change for each respective gene is normalized and compared with mock infection. Data shown are representative of at least three independent experiments performed in triplicate. Error bars indicate SD. *$p < 0.05$; **$p < 0.01$; ***$p < 0.001$; ****$p < 0.0001$.

ALI-HNECs, air-liquid interface-human nasopharyngeal epithelial cells; ALI-HBECs, air-liquid interface-human bronchial epithelial cells; CFU, colony forming unit;TEER, transepithelial electrical resistance; hpi, hours post infection; IL, interleukin.

of *P. aeruginosa* in mouse lungs dropped continuously and were cleared from mouse lungs by day 7 post infection, whereas *N. subflava* continue to demonstrate increased bacterial loads at day 7 post infection which remain high at day 14 post infection. These findings demonstrate *N. subflava's* ability to persist for a prolonged time period, whereas *P. aeruginosa* inhalation, following an acute response, is cleared more rapidly (Figure 3C). *N. subflava* exhibits distinct bronchiolar epithelial damage in comparison with *P. aeruginosa* suggestive of distinct pathology (Figure S4). Assessment of *N. subflava* load, measured by culture of lung homogenates, reveal the establishment of infection in the mouse lung by day 4 and up to day 14 (Figure 3C). To further confirm successful lower airway infection, FISH analysis detected *N. subflava* within infected mouse lung parenchyma up to day 14 post infection (Figure 3D). *N. subflava* infection induced macroscopic lung tissue damage, including bleeding and lobar inflammation on day 4 (Figure 3E). Acute inflammation was confirmed by Giemsa staining of bronchoalveolar lavage fluid (BALF), demonstrating predominantly alveolar macrophages initially (day 0) followed by neutrophilic infiltration (day 2) (Figure 3F). Bronchioalveolar infection and tissue damage induced by *N. subflava* were evident from H&E staining of mouse lungs: bronchiolar damage and pro-inflammatory immune cell infiltration into alveolar spaces were observed between days 2 and 7 post infection, peaking at day 4, followed by recovery at day 14 (Figures 3G and 3H). The immune-inflammatory response *in vivo* was further confirmed by flow cytometry, revealing an acute (early) inflammatory phase marked by neutrophilic (Ly6G+ F4/80− CD45+) and NK cell (NK1.1+ CD19− CD45+) infiltration followed by an adaptive (late phase) response characterized by T helper cells (CD4+ CD3+), cytotoxic T cells (CD8+ CD3+), macrophages (F4/80+ Ly6G− CD45+), and B cells (CD19+ NK1.1− CD45+) consistent with acute respiratory infection (Figure 3I).

Lung transcriptomics demonstrates immunoinflammatory functional gene clusters following *N. subflava* infection *in vivo*

Having observed *N. subflava* infection and its immunoinflammatory consequence *in vivo*, we next sought to characterize the post infection lung transcriptomic response. RNA sequencing of infected mouse lung was performed over a 14-day infection course, revealing dynamic change (Figure 4A). Principal component analysis (PCA) identified major shifts in gene expression

CellPress
OPEN ACCESS

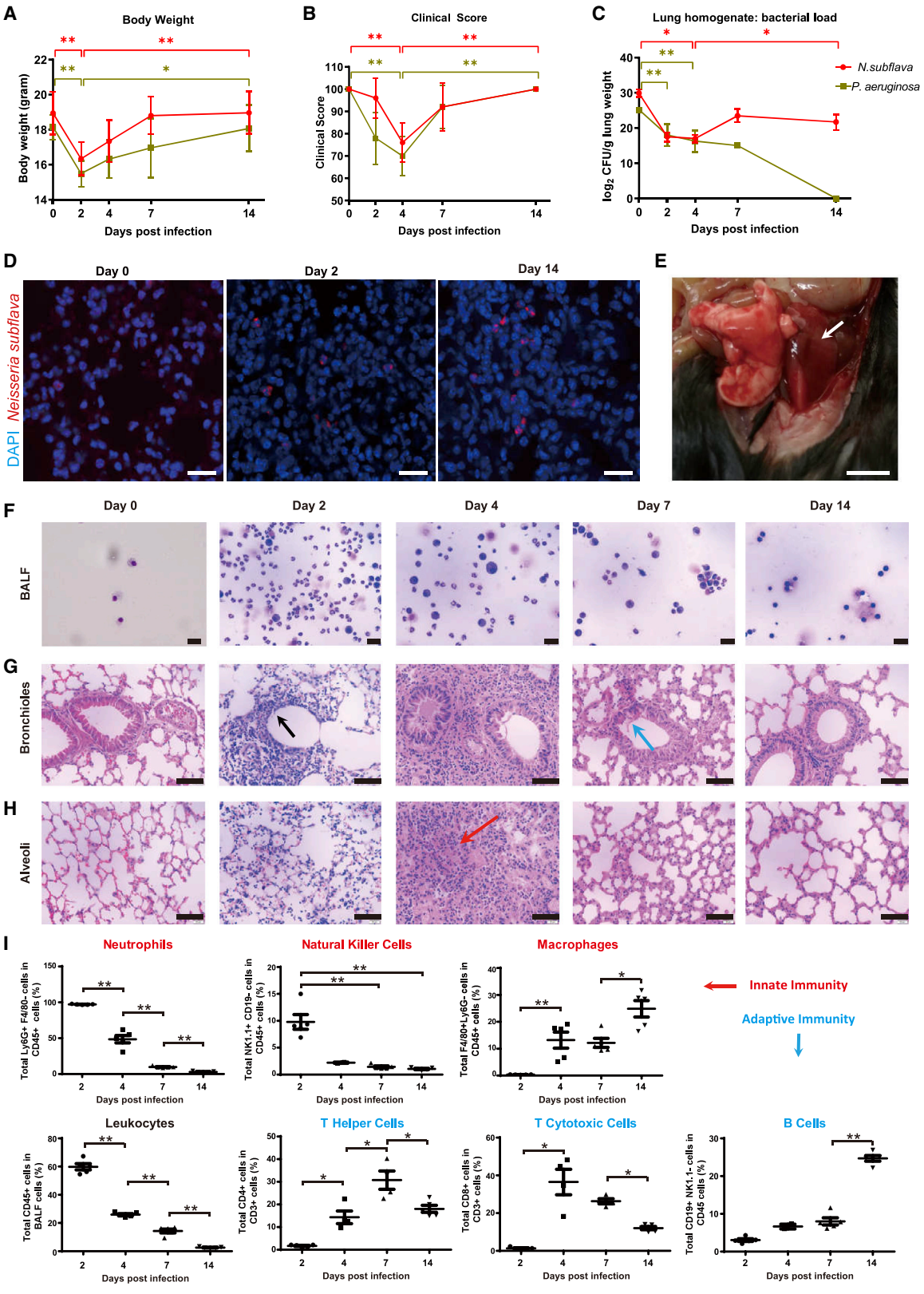

(legend on next page)

between day 0 and day 2 post infection, followed by return to baseline and relative quiescence by day 7 (Figure 4B). This was followed by a delayed but marked shift in gene expression during recovery at day 14 (Figure 4B). To better define functional changes, we clustered the observed differential gene expression patterns according to enriched functional pathways, revealing seven ''functional'' clusters (Figure 4C). Early phase changes were characterized by immune cell function, infiltration, and antimicrobial responses, which peaked at day 2, followed by an inflammatory/oxidative stress response at day 4 (Figure 4C). These changes corroborate our macroscopic, microscopic, and flow cytometry data, where at day 2, an antibacterial response ensues, marked by infiltration of neutrophils (Figures 3F, 3H, and 3I), confirmed by gene expression patterns of hypercytokinemia, phagosome formation, and pattern recognition receptor activity (Figure 4C) reflected in an upper right shift in the PCA compared with day 0 (Figure 4B). At days 4 and 7, the acute host response to bacterial infection was reduced, marked by lower neutrophil infiltration (Figures 3F and 3I), and a curtailed immune response, most notably at day 7 (Figure 4C). Interestingly, day 7 gene expression was comparable with baseline (day 0), in the number of differentially expressed genes (DEGs) (Figure 4A) and reflected by a shift toward baseline in PCA and functional pathway analysis, respectively (Figures 4B and 4C) potentially indicative of immune tolerance toward *N. subflava* at this later time point. Importantly, increased *N. subflava* load in mouse lung was observed, but in the absence of excessive host immune responses at this later time point (Figure 3C). In contrast, host responses at day 14 demonstrate a highly altered profile relative to both baseline (day 0) and day 7 (Figure 4A), suggestive of an airway remodeling response (Figure 4C), concomitant with sustained levels of *N. subflava* in the airway (Figure 3C). Therefore, taken together, intratracheal exposure *in vivo* leads to a sustained presence of *N. subflava* in the airway and an altered host immune response characterized by an initial pro-inflammatory profile, oxidative stress response, and macroscopic tissue damage (days 2 and 4), followed by immune quiescence (day 7), and subsequent airway remodeling (day 14). Late-stage gene expression was marked by significant shifts from immune function to airway remodeling involving gap junction and endothelin signaling, suggesting a potentially prolonged immunopathology linked to airway damage following initial *N. subflava* infection (Figure 4C). Interestingly, patterns observed from *N. subflava* infection were distinct from those observed following *P. aeruginosa* infection when transcriptomes are directly compared (Figure S4G). PCA reveals diverse lung transcriptomes across the 14-day infection course for both organisms. Lung transcriptomes following *P. aeruginosa* infection formed a separate cluster to those following *N. subflava* infection and demonstrate a major shift between days 0 and 2 with marginal change from day 4 onward (Figure S4H). Temporal expression of key inflammatory genes indicates acute inflammatory changes identified in our ALI models such as IL-6, TNF, CCL2, and CXCL10 (Figure 2D) were elevated following infection by both organisms; however, changes associated with *N. subflava* were two to three orders of magnitude larger than the baseline, compared with moderate upregulation observed with *P aeruginosa* (Figure S4I). Taken together, although both microbes induce vastly diverse pulmonary responses, *N. subflava* appears more immunogenic, triggering a more intense inflammatory response following acute infection, followed by a prolonged airway remodeling effect (Figures S4G–S4I).

N. subflava induces a pro-inflammatory pulmonary metabolipidome

The overall lung sampling strategy for metabolipidome analyses is illustrated and includes sampling from a control (uninfected) group (H) (Figure 5A). Paired tissue sampling from the ipsilateral lobe of the infected lung was performed that included areas demonstrating macroscopic infection (ID, infected [diseased]) paired to uninfected areas (IH, infected [healthy]) (Figure 5A). Analysis of the mouse metabolipidome reveals that *N. subflava*-infected mice—even in apparently (macroscopically) uninfected regions, demonstrate distinct immunoinflammatory profiles characterized by upregulated coenzyme Q10 biosynthesis, pyrimidine ribonucleotide biosynthesis, and nitric oxide signaling, mirroring innate immune signatures of the transcriptome and suggesting an inflammatory response at the infection site and surrounding regions (Figures 5 and S5A–S5E). In comparing uninfected (H) and infected (ID) mice, 113 significantly dysregulated metabolites and lipids were identified, at fold changes $\geq$1.5, including several involved in immune regulation, immunometabolism, second messaging, and plasma membrane-mediated cell signaling (Figures 5B, 5C, and S6E; Table S3). Through connectivity network analyses, we assessed for interrelationships between the transcriptomic gene clusters (Figure 4C) and the dysregulated metabolipidome (Figures 5B–5D). This revealed activation of lipid-associated metabolic pathways related to itaconic acid, oleic acid, and ceramide (d34:2 and d34:0) biosynthesis, following *N. subflava* infection. In addition, perturbations in cell signal transduction linked to nitric oxide signaling and

Figure 3. Intratracheal delivery of *N. subflava* induces bronchioalveolar infection and immunoinflammatory responses *in vivo*

(A and B) *N. subflava* (red) and *P. aeruginosa* (green) were delivered intratracheally to C57BL/6 mice on day 0, and the mice were monitored for (A) body weight and (B) clinical score change.

(C–F) (C) Bacterial load in lung homogenates following growth on chocolate agar at time points indicated, with error bars indicating SD. Successful infection was confirmed by (D) fluorescent *in situ* hybridization (FISH) (Fanger et al., 1997) detection of *N. subflava* in mouse lung biopsies (scale bars, 20 μm), (E) macroscopic inflammatory damage in mouse lobar tissue at day 4 post infection (white arrow) (scale bars, 1 cm), and (F) Giemsa staining of bronchoalveolar lavage fluid (BALF) cellular content at indicated time points that illustrate an abundance of pro-inflammatory cells at days 2 and 4 post infection, respectively (scale bars, 20 μm).

(G and H) H&E staining of lung tissue from *N. subflava*-infected mice demonstrate inflammation and tissue damage in the (G) bronchioles and (H) alveoli. Scale bars, 150 μm. At day 2 post infection, bronchiolar epithelial damage is observed (black arrow) followed on day 4 by alveolar infiltration and edema (red arrow). Bronchiolar epithelial damage persists to day 7 post infection (blue arrow).

(I) Flow cytometry of immune cells from infected mouse BALF displays the presence of a pro-inflammatory response at early time points (days 2 and 4 post infection) with adaptive immune responses at later time points (days 7 and 14 post infection). *$p < 0.05$ and **$p < 0.01$. The inter quartile range (IQR) of measurements is indicated with bisecting lines representing the median and whiskers representing 1.5 times the IQR.

CellPress
OPEN ACCESS

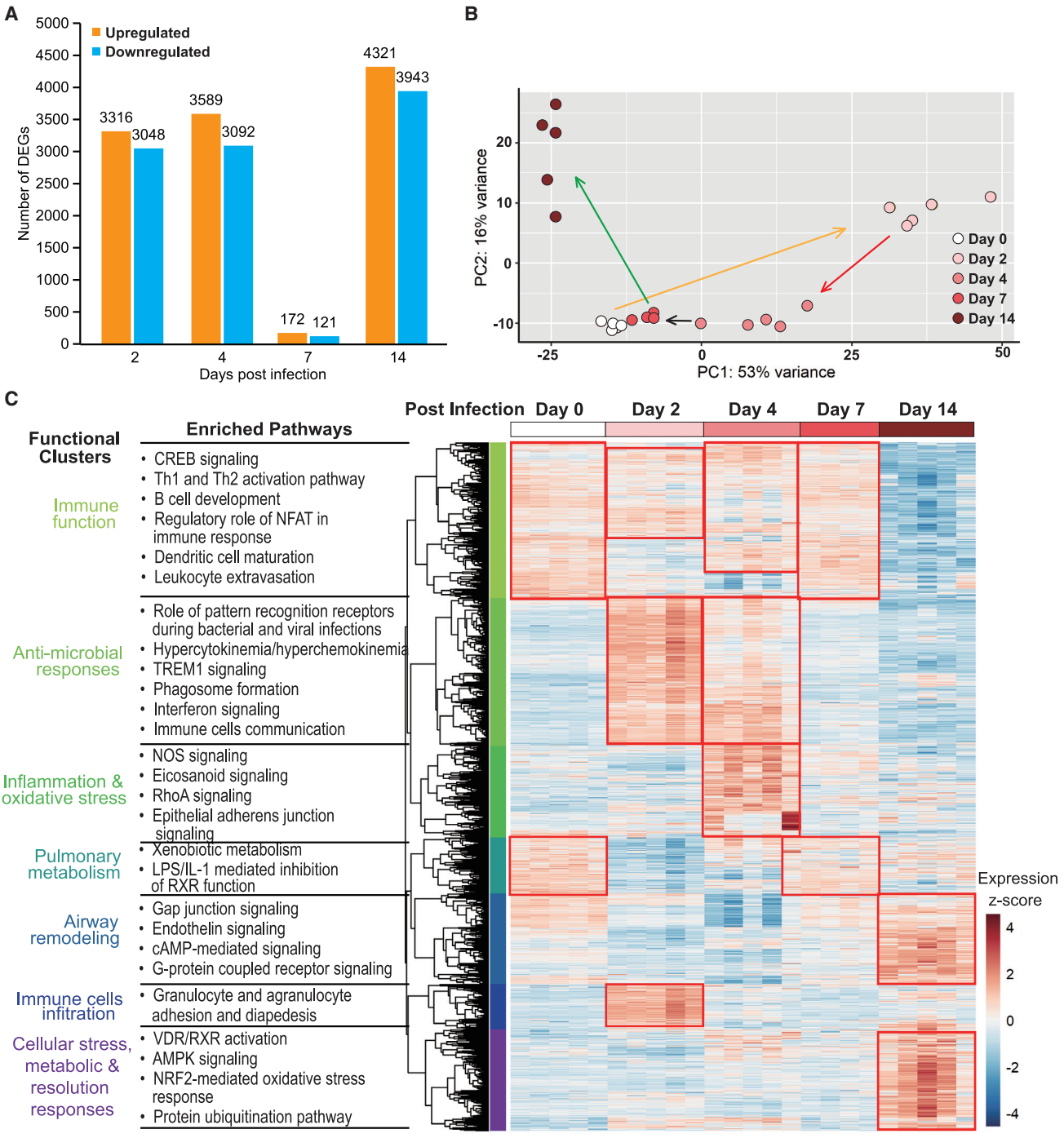

Figure 4. Mouse lung transcriptomics demonstrate functional gene clusters *in vivo* in response to *N. subflava* infection

(A) RNA sequencing of infected mouse lung at the indicated time points following *N. subflava* infection reveals change to differentially expressed genes (DEGs) across the 14-day course of infection.

(B) Principal component analysis (PCA) of mouse lung transcriptomes across the 14-day course of infection demonstrates shifts in host response. Colored arrows indicate directionality of the relative transcriptomic change observed.

(C) Heatmap indicating seven functional gene clusters from mouse lung transcriptomes illustrating significantly DEGs and respective enriched pathways in response to *N. subflava* infection. All illustrated changes are presented relative to control (uninfected) mice at day 0 with red coloration (including boxes) indicative of gene-pathway upregulation and blue coloration downregulation. All experiments were performed using n = 5 mice for each respective time point.

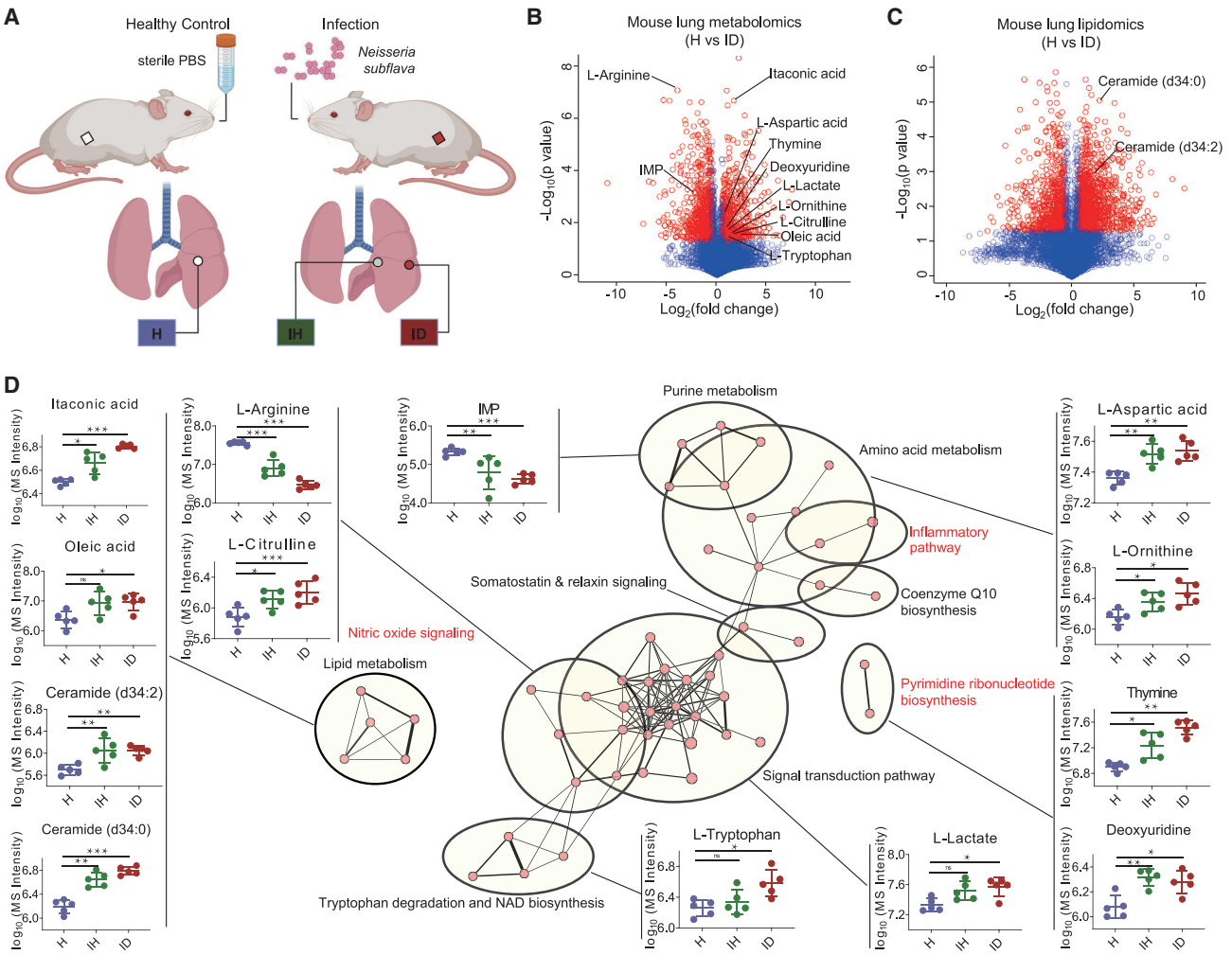

Figure 5. *N. subflava* induces pulmonary inflammation *in vivo* through the metabolipidome

(A) Pictorial overview of the sampling strategy used for metabolipidome analysis following *N. subflava* infection: C57BL/6 mice were inoculated intratracheally with *N. subflava* (infection arm) or sterile phosphate buffered saline (PBS) (control arm). Paired tissue sampling from the ipsilateral lobe of resected lung was performed from the healthy (control arm) (H: white circle) and infected arm. Infected arm sampling was performed from areas demonstrating macroscopic infection (ID: red circle) and paired with uninfected areas from the ipsilateral lobe (IH: gray circle).

(B and C) Volcano plots summarizing (B) metabolomic and (C) lipidomic analyses comparing uninfected healthy mouse lung (H) (control) with *N. subflava*-infected mouse lung (ID). Significant metabolite and lipid differences are labeled.

(D) Connectivity networks from the lung transcriptome through pathway enrichment analyses and differentially expressed genes (DEGs) are linked to lung metabolipidome profiles. A single node represents a single enriched pathway, and nodes with similar function are illustrated as larger clusters with their biological function annotated. Representative metabolites or lipids from the metabolipidome are linked to the transcriptome with specific comparisons illustrated between H, IH, and ID as illustrated. *$p < 0.05$, **$p < 0.01$, and ***$p < 0.001$.

H, healthy (uninfected control); IH, infected (healthy); ID, infected (diseased); IMP, inosine 5′-monophosphate.

inflammation were observed, whereas metabolic pathways related to redox homeostasis and metabolism of several macronutrients including amino and nucleic acids were altered. Taken together, metabolipidome analyses confirmed significant shifts in metabolic and immune responses toward a pro-inflammatory state in *Neisseria*-infected lung tissue independent of macroscopic appearance (Figure 5A: IH and ID). Consistent with RNA sequencing data, the pro-inflammatory profile of the metabolipidome further underscores the immunopathogenic potential of *N. subflava* implicating it in lung damage seen in our murine infection model.

Systemic change to the metabolipidome is detectable in *Neisseria*-dominant bronchiectasis

Having characterized transcriptomic and metabolipidomic lung tissue responses to *N. subflava*, we next assessed the systemic metabolipidome (using mouse serum) revealing infection-related profile shifts, marked by an altered lipidome as early as day 2 post infection, consistent with lung transcriptomes (Figures 4, 6, and S5F–S5J). Mice exhibited two distinct metabolipid clusters defining dynamic change over the course of *N. subflava* infection (Figure 6A). To link lung alteration to the observed systemic change, we next performed weighted gene co-expression

CellPress
OPEN ACCESS

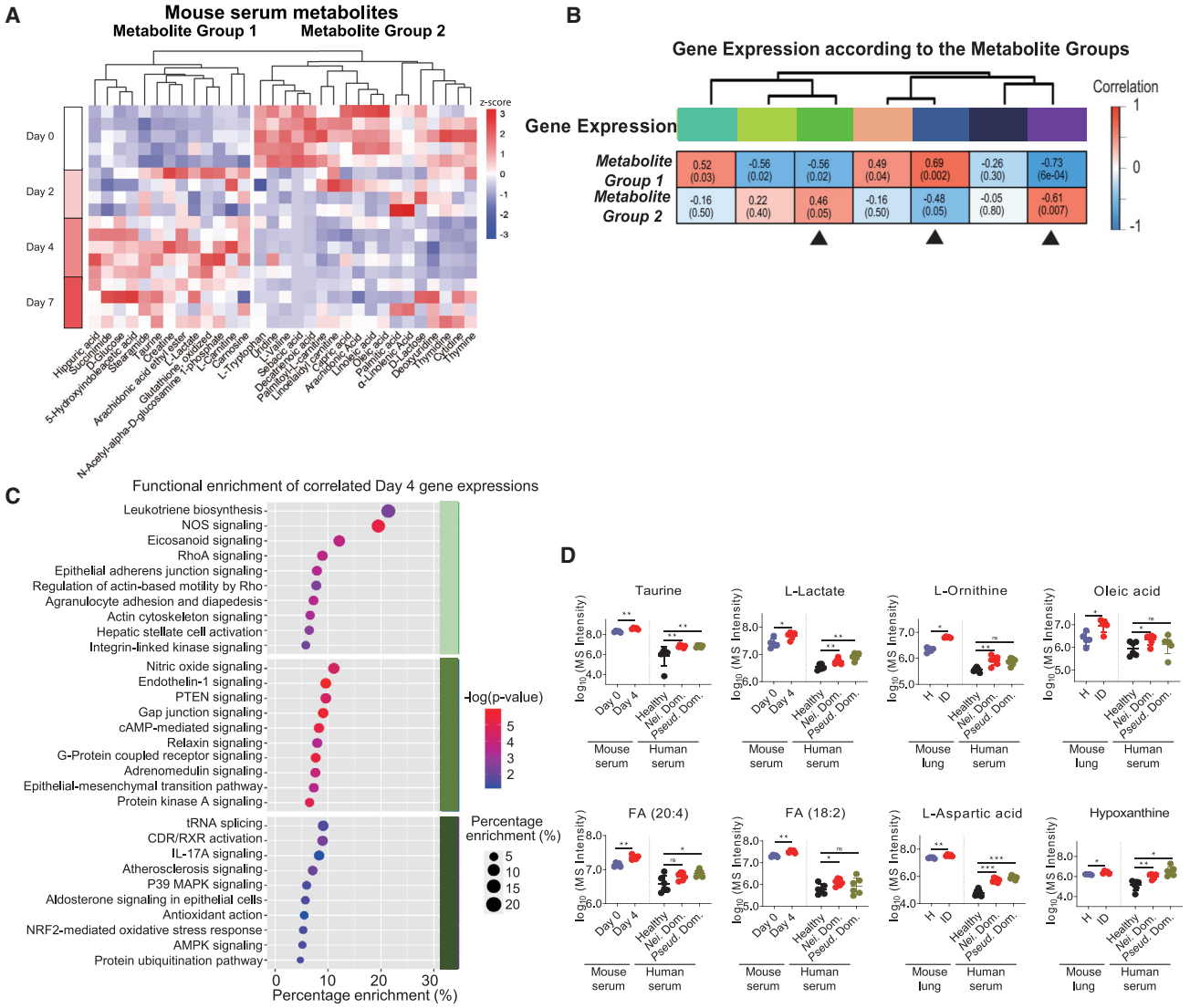

Figure 6. *N. subflava* induces detectable systemic change to the metabolipidome in *Neisseria*-dominant bronchiectasis

(A) Hierarchal clustering of altered mouse serum metabolomic profiles into two groups following *N. subflava* infection performed at day 0 (pre-infection) and days 2, 4, and 7 post infection as illustrated. Red coloration indicates higher concentrations, whereas blue coloration indicates lower concentrations of the respective metabolites.

(B) Weighted correlation network analysis (WGCNA) of mouse lung transcriptomes and serum metabolipidomes post *N. subflava* infection reveals three gene modules (black arrows) that correlate with the previously derived serum metabolite groupings. Red coloration of the respective boxes indicates a positive correlation, whereas blue coloration indicates a negative correlation. Correlation coefficients (R) and respective p value (in parenthesis) are indicated.

(C) Summary of top 10 enriched pathways (predicted by ingenuity pathway analysis [IPA]) from each of the three correlated transcriptomic gene modules to serum metabolomic profiles in *N. subflava*-infected mice. The x axis (percentage enrichment) denotes the proportion of serum metabolites involved in a particular pathway, and dot coloration indicates log-transformed p values (i.e., red coloration correlates to lower and more significant p values).

(D) Summary of key metabolites and lipids from the systemic metabolipidome demonstrating concurrence between mouse and human serum. *N. subflava*-infected mice at days 0 (pre-infection) and 4 (post infection) are indicated and compared with serum from non-diseased (healthy) individuals (n = 6) and *Neisseria*-(n = 6) or *Pseudomonas*-dominant bronchiectasis (n = 6). *p < 0.05, **p < 0.01, and ***p < 0.001. The inter quartile range (IQR) of measurments is indicated with bisecting lines representing the median and whiskers representing 1.5 times the IQR. FA(20:4): arachidonic acid (20:4, n −6); FA(18:2): 18:2 linoleic acid;
H, healthy (uninfected control); IH, infected (healthy); ID, infected (diseased); Nei. Dom, *Neisseria*-dominant bronchiectasis; Pseud. Dom, *Pseudomonas*-dominant bronchiectasis.

network analysis (WGCNA) on mouse lung transcriptomes that identified seven distinct gene modules, three of which significantly correlated with our derived serum clusters (Figure 6B). Functional enrichment of these modules (incorporating the systemic metabolipidome profiles) identified key pathways linking the transcriptome with the metabolipidome. *N. subflava* lung exposure leads to metabolic shifts associated with activation of pro-inflammatory signaling pathways including leukotriene biosynthesis, nitric oxide, and eicosanoid signaling (Figure 6C). Pathways related to airway remodeling, such as endothelin-1,

epithelial adherens, and actin cytoskeleton signaling were also associated with serum metabolomic clusters, as were Phosphatase and Tensin homolog (PTEN), gap junction, and relaxin signaling, further implicating an airway remodeling response (Figure 6C).

To translate mouse findings to *Neisseria*-dominant bronchiectasis (Figure 1), we performed systemic metabolipidome analyses using human serum obtained from non-diseased (healthy) controls and individuals from the Asian arm of the CAMEB cohort with *Neisseria*- and/or *Pseudomonas*-dominant bronchiectasis, the latter an established bronchiectasis pathogen (Finch et al., 2015). Interestingly, overlapping profiles were observed but distinct from healthy individuals (controls) (Figures S6A–S6D). Eighty-one metabolipids were identified in *Neisseria*-dominant bronchiectasis (Figure S6E), of which 8 were selected for further validation based on correlations with mouse serum (i.e., taurine, L-lactate, and fatty acids FA[20:4] and FA[18:2]) and mouse lung (L-ornithine, oleic acid, L-aspartic acid, and hypoxanthine) profiles, respectively (Figure 6D). The strong validation between human serum profiles in *Neisseria*-dominant bronchiectasis and those obtained in the murine infection model suggest shared mechanisms of *Neisseria*-associated infection (Figure 6D). Further confirmation of the clinical value to our findings is the comparable results between *Neisseria*- and *Pseudomonas*-dominant microbiomes, the latter an established bronchiectasis pathogen associated with poor clinical outcome (Aliberti et al., 2016; Finch et al., 2015; Figure 6D). The potential influence of the dual presence of *Neisseria* and *Pseudomonas* (to differing extents) was assessed (Figure S7) and revealed important subtle influences on their respective systemic metabolipidomic profiles suggestive of differing pathogenic mechanisms in individual patients related to a combination of colonization and respective relative abundance. Therefore, employing a systems biology approach combining human and mouse sampling, we demonstrate that *Neisseria* spp. induces inflammatory and airway remodeling responses with strong measurable clinical correlation that is comparable with the established bronchiectasis pathogen *P. aeruginosa*.

Metagenomic surveillance of *Neisseria* in chronic respiratory disease and the home environment in bronchiectasis

Our identification and characterization of *N. subflava* as an airway pathobiont in bronchiectasis leads to the consideration of *Neisseria* spp. as pathobionts in other chronic respiratory diseases. To build on our targeted 16S rRNA sequencing approach (Figure 1), we employed shotgun metagenomics to evaluate *Neisseria* spp. in bronchiectasis, severe asthma (SA), and chronic obstructive pulmonary disease (COPD) including healthy (non-diseased) individuals recruited from Asia (SK-KL) and the United Kingdom (DD), respectively (Figure 7A). We confirmed the presence of *Neisseria* species (including *N. subflava*) in all diseased groups with increased abundance noted in individuals recruited from our SG-KL cohort. In contrast, non-Asians, though exhibiting *Neisseria* spp. in all groups, had comparatively less abundance, a feature consistent with prior 16S rRNA findings in bronchiectasis (Figures 1 and 7A). Although *Neisseria* spp. are considered upper airway commensals, except for established pathogenicity in the setting of meningitis and gonorrhea, our findings point toward potential clinical association upon airway exposure in respiratory disease. Prior metagenomic analysis from our group highlights the potential of the home environment as a source of microbial exposure (Mac Aogáin et al., 2020; Tiew et al., 2020). We therefore prospectively investigated ten homes, selected based on individuals demonstrating *Neisseria*-dominant bronchiectasis, and performed metagenomic evaluation of microbial content in the air, in airway, and on environmental surfaces in their residence. A significant *Neisseria* spp. presence was confirmed in host airways and on associated inhaler devices. Interestingly, *Neisseria* spp. (including *N. subflava*) was identified on air conditioning filters, fans, and indoor air samples, in contrast to outdoor air (sampled on the balcony or outside home windows) concurrently. Outdoor air metagenomes revealed minimal *Neisseria* detection, suggesting the indoor home environment as a potential exposure source of this pathobiont (Figure 7B).

DISCUSSION

Here, employing a bedside-to-bench translational approach leveraging *in-vitro*, *in- vivo*, and *ex-vivo* approaches in human and animal models, the integration of next-generation sequencing and systems biology demonstrates that *Neisseria* species and *N. subflava*, in particular, represent a pathobiont in bronchiectasis. *Neisseria*-dominant microbiome profiles were detected at variable frequency based on geographic origin and relate to poor clinical outcomes in bronchiectasis. *N. subflava*, cultured from respiratory specimens, were subjected to primary human epithelial and mouse infection models to reveal its pathogenicity. Systems biology including transcriptomics, metabolomics, and lipidomics characterized the immune-inflammatory response *in vivo* which was validated in *Neisseria*-dominant bronchiectasis. These data reveal comparable features with those of *Pseudomonas*-dominant disease, an established bronchiectasis pathogen. Metagenomics applied to specimens from other respiratory diseases, including SA and COPD, demonstrates the broader significance of detecting *Neisseria* species *in vivo*, and the home environment potentially represents a key source of exposure.

Applying microbiome-based analysis to stratify disease subphenotypes is gaining traction across translational studies and, in bronchiectasis, demonstrates that the poor prognosis associated with *Pseudomonas* and *Veillonella* dominance (Rogers et al., 2014a, 2014b). Our current work builds significantly on these early observations, by identifying geography as an important microbial determinant, utilizing carefully curated and "matched" patient cohorts. We demonstrate a bronchiectasis microbial phenotype characterized by *Neisseriaceae* of strong clinical relevance. Culture followed by molecular characterization leads to the identification of *N. subflava* by whole-genome sequence analysis, followed by confirmation of its presence in the lower airways in bronchiectasis by FISH. *Neisseria* spp. represent a significant component of the human microbiome, constituting part of the "core microbiome" in the oral cavity (Donati et al., 2016). Traditionally, "non-pathogenic" genera remain poorly characterized with regard to their pathogenicity, with the notable exception of limited reports in bronchiectasis (Liu et al., 2015). *N. subflava* impacted tight junctions and cell barrier integrity in

CellPress
OPEN ACCESS

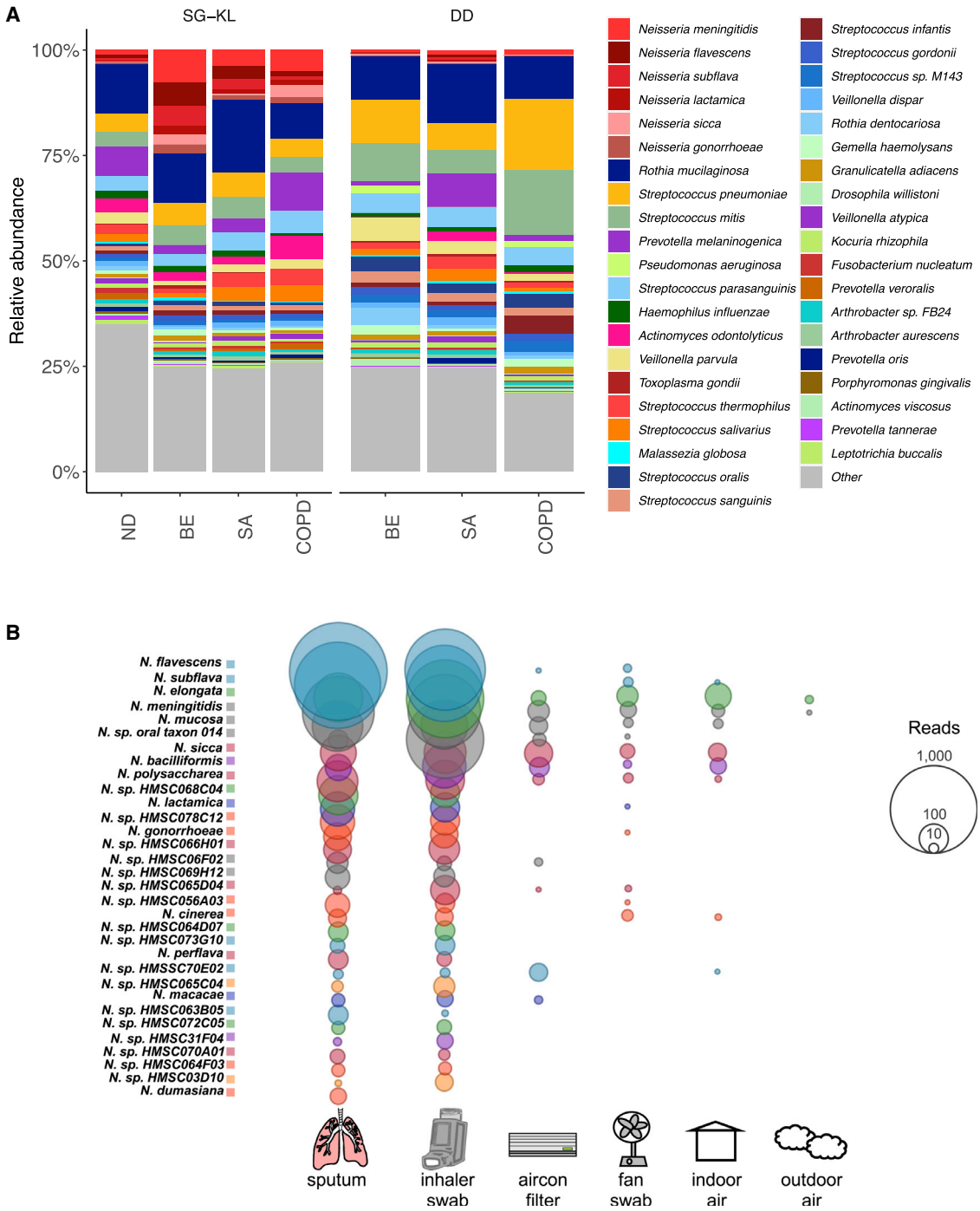

Figure 7. Metagenomic surveillance of *Neisseria* spp. in respiratory disease and the home environment of *Neisseria*-dominant bronchiectasis

(A) Metagenomic species level analysis indicating the relative abundance of the top 40 microbes in non-diseased (healthy) controls (n = 8) and individuals with respiratory disease, including bronchiectasis (BE) (n = 12), severe asthma (SA) (n = 8), and chronic obstructive pulmonary disease (COPD) (n = 8). Recruited individuals are illustrated based on the country of origin where SG-KL reflects recruits from Singapore-Kuala Lumpur, Malaysia (left), and DD individuals from Dundee, Scotland (right). The various *Neisseria* species are indicated at the top of each respective barplot to highlight their variable abundance across disease states and by geographic region. All taxa are colored according to the legend.

(B) Metagenomic analysis of the home environment in n = 10 *Neisseria*-dominant individuals with bronchiectasis reveals *Neisseria* spp. in indoor air and home surfaces. Metagenomic sequencing of outdoor and indoor air, individual sputum, and swabs of an accompanying inhaler device and surfaces in the home environment including aircon filter and fan were performed, and top 40 detected *Neisseria* species (and relative abundance) are illustrated. Bubble size corresponds to the number of reads assigned to each respective taxon.

our primary human nasopharyngeal and bronchial cellular models, features previously observed only for overt pathogenic members of the *Neisseriaceae*, suggestive of invasive potential (Sutherland et al., 2010). Immunological assessment reveals increased expression of IL-6 and IL-8 with markedly enhanced CCL2 (MCP-1), all features of immune dysregulation in bronchiectasis (King, 2018; McShane, 2019). Induction of CXCL10 (IP-10) is noteworthy, given its increased expression in response to pathogenic *N. meningitidis* (and in fulminant meningitis) possibly due to conserved antigenic moieties between members of the *Neisseriaceae* (Ovstebø et al., 2008). Critically, microbiome-based signatures in bronchiectasis exhibit demonstrable association with host immune responses: *H. influenzae*-dominance exhibits increased matrix metalloprotease-2 and -8 (MMP2 and MMP8) relative to *Pseudomonas*-dominance, whereas overall taxonomic diversity relates to IL-1β and IL-8 expressions. Increased microbial richness further predicts improved clinical outcomes and reduced inflammatory signaling (Rogers et al., 2014a; Taylor et al., 2015). Our work further supports such association between individual microbiome profiles and airway immunological signatures, here in relation to airway *Neisseria*, lending increased credence to the emerging role of upper airway bacterial migration in shaping lower airway immunology (Dickson et al., 2017; Segal et al., 2016; Wu et al., 2021).

Animal models of infection are described for *Neisseria*; however, these largely focus on *N. meningitidis* (Weyand, 2017). Dedicated studies of "non-pathogenic" *Neisseria* in the mouse remain lacking. Further, no animal model representative of bronchiectasis is currently available, representing a challenge to establishing causality in this field. The inherent disease heterogeneity and chronic progressive nature of bronchiectasis (varying between individuals) makes modeling this disease *ex-vivo* challenging and a key knowledge gap in the field. Current approaches remain inadequate in reproducing the *in vivo* state in bronchiectasis, limiting our experimental options, despite infection remaining central to its pathogenesis (Flume et al., 2018). Here, we demonstrate, in an acute intratracheal mouse model, that *N. subflava* promotes bronchio-alveolar infection, significant pulmonary inflammation and tissue destruction. Although *Neisseria*-associated alveolar infection clears within days, bronchiolar infection persists in an inimitable pattern distinct from that seen in *S. pneumoniae* or *P. aeruginosa* pulmonary infection (Kadioglu et al., 2000; Kukavica-Ibrulj et al., 2014). Our murine model identifies an early innate immune response characterized by neutrophilic and NK cell infiltration into lung parenchyma, followed by a late adaptive phase involving T helper cells, cytotoxic T cells, and B cells accompanied by persistence of *N. subflava*. Taken together, these results implicate *N. subflava* in triggering innate and adaptive immunity in line with other pathogens: a classical phagocytic phase followed by lymphocytic response. Recent work assessing the episodic aspiration of upper airway commensals similarly investigated their ability to trigger airway immune responses (Wu et al., 2021). Given strong associations between microbiology and bronchiectasis phenotypes, more refined chronic disease models may require incorporation of specific microbial exposures—as is the case for other model systems such as the use of *H. influenzae* in COPD models (Gaschler et al., 2009) or respiratory syncytial virus (RSV) in asthma (You et al., 2006). Although our murine model is unlikely to be completely reflective of the clinical situation in all patients, we note that the bronchiolar inflammation observed points to *Neisseria*-specific mechanisms of inflammation and remodeling (defined by our transcriptomics/metabolomics) and is distinct to that of a *P. aeruginosa* challenge. This may direct the future development of murine bronchiectasis models, at least for a subset of patients. The relatively sustained infective potential and extensive macro- and microscopic pulmonary damage observed in our model likely reflect our direct inoculation strategy, mimicking deeper and prolonged lower airway exposure to *N. subflava* compared with the upper airway aspiration of commensal *Neisseria* spp.

To characterize the host response, transcriptomics, performed longitudinally over the course of *N. subflava* infection, closely reflected the immune response observed in our mouse model. Enrichment of antibacterial and phagocytic response signals was observed early, which progressed to an inflammatory and oxidative stress response, before emergence of an airway remodeling signature. Although bronchiectasis is primarily a neutrophilic disease, emerging work implicates allergic sensitization in disease pathogenesis in subgroups (Mac Aogáin et al., 2019). Enrichment of the endothelin pathway, as part of a broader functional airway remodeling, potentially suggests a role for hypersensitization associated with *N. subflava* (Gregory et al., 2013).

Metabolipidomic approaches, accompanied by validation, provide scope for biomarker discovery and refined stratification of subphenotypes in respiratory disease (Wheelock et al., 2013). Having established *N. subflava* pathogenicity *in vivo*, we next identified a dysregulated metabolipidome, validated in human disease, and characterized by significant immunometabolic reprogramming implicating arginine and tryptophan metabolism and increased ceramide (Bronte and Zanovello, 2005). Host defense against respiratory pathogens such as *P. aeruginosa* is characterized by ceramide release, due to lipid raft remodeling, a common site for pathogen-host signaling (Grassmé et al., 2003). Importantly, this represents a potential mechanism of mucosal invasion, employed by *N.* gonorrheae, which may serve as an important signaling platform for interaction with commensal *Neisseriaceae* (Grassmé et al., 1997). Systemic murine metabolomes, sampled serially following *N. subflava* infection, reveal metabolic clusters that upon functional integration with transcriptomes identify key analytes of interest that were validated with human serum from *Neisseria*- and *Pseudomonas*-dominant bronchiectasis. Major markers include arachidonic, linoleic, and oleic acids, whose alteration is consistent with an infection-driven fatty acid profile and indicates a leukotriene-associated response. These were accompanied by taurine, lactate, ornithine, aspartic acid, and hypoxanthine, all linked to oxidative stress (Schmidt et al., 2001; Wenzel, 1997).

Given the clinical relevance of *Neisseria*-dominant microbiomes in bronchiectasis, we explored other chronic respiratory diseases including SA and COPD. We confirmed detection and high relative abundance of *Neisseria* spp. across these diseases, particularly in individuals recruited in Asia, suggesting clinical relevance beyond bronchiectasis. Geographic variability in bronchiectasis airway microbiology is not limited to *Neisseria*, as significant differences in the prevalence of pathogens are observed

including *H. influenzae*, the driving factors of which are multifactorial including host, environmental, exposure, and climatic influences (Chalmers and Chotirmall, 2018; Chotirmall et al., 2017; Rogers et al., 2014b).

Our group has previously applied metagenomic profiling to establish associations between microbial exposure in the indoor environment and respiratory disease outcomes (Mac Aogáin et al., 2020; Tiew et al., 2020). Using similar approaches, we sought to identify potential sources of *Neisseria* spp. in the home environment of bronchiectasis patients. The presence of *N. subflava*, among other members of the *Neisseriaceae*, was detectable in the homes of patients with bronchiectasis highlighting the organism's ability to persist in the home and represent an environmental source for repeated exposure. These observations suggest that microbial signatures in the home may influence human microbiome profiles and potentially clinical course and outcomes. Importantly, the nature and directionality of such environmental microbial exposures (i.e., environment influencing host or vice versa) and its direct impact on bronchiectasis and other respiratory diseases requires further exploration in controlled studies.

Our study has several strengths: well-matched human cohorts across geographic locations, use of a broad range of primary human cellular and animal infection models, and application of a variety of next-generation sequencing and systems biology approaches to characterize *Neisseria* as pathobionts in bronchiectasis.

Limitations of the study

Although we successfully isolated *N. subflava* from respiratory specimens in *Neisseria*-dominant microbiomes using established culture methodologies, our approach may have biased detection toward non-fastidious species and selectively favored the culture of *N. subflava*. Broader metagenomic sequencing of airway samples or the application of advanced "culture-omics" may better serve in determining if other *Neisseria* spp. are implicated in bronchiectasis (Whelan et al., 2020). Thus, although our work highlights the potential pathobiont role of airway *Neisseriaceae*, we acknowledge that they likely represent one of several commensal airway taxa implicated by a growing body literature to be involved in microbial host interaction as part of complex airway microbial consortia (Dickson et al., 2017; Rigauts et al., 2022; Segal et al., 2016; Wu et al., 2021). In identifying other geographically distinct taxa, we applied LEfSe analysis that corroborated our main finding with respect to *Neisseria* abundance. However, it is clear that the identification of discriminant taxa may give differing results based on analytical methods chosen for assessment of compositional data (Nearing et al., 2022). Novel approaches for mitigating these challenges such as analysis of compositions of microbiomes with bias correction (ANCOM-BC) continue to be developed for more robust microbiome comparisons (Lin and Peddada, 2020). We did not directly assess bacterial load using qPCR, which would have provided insight to bacterial burden, a factor that could have an important role in *Neisseria*-mediated airway pathology. Our work did not include any therapeutic intervention targeting *Neisseria*-dominant microbiomes, and hence, clinical benefit of targeting *Neisseria* in bronchiectasis remains to be determined. Future clinical validation through well-designed intervention studies will be necessary. Although we took great effort to match Asian and European patients, geographic confounders potentially remain. These include exacerbations, use of corticosteroids and antibiotics, and microbiological culture results. This was partly due to a clinical matching criterion based on the bronchiectasis severity index (BSI) score which allows for variable phenotypes within patients of similar scores and the known geographic heterogeneity of this disease (Chandrasekaran et al., 2018; Dhar et al., 2019). This issue was mitigated to some extent as *Neisseria*-associated clinical phenotypes were largely assessed in Asian patients in this work. Related to this, our analysis of *Neisseria*-associated clinical relationships among Europeans was limited by the low numbers of *Neisseria*-dominant patients in the Dundee cohort. This, however, does not exclude the possibility of such phenomena occurring among patients from this region that may require broader sampling to detect. Finally, our use of human bacterial strains in a murine model likely triggered heightened immune responses, which should be considered in interpreting our data.

In summary, we present clinical and experimental data indicative of *Neisseria* spp. as unrecognized lung "pathobionts" in bronchiectasis and other respiratory diseases representing a "targetable" microbial trait of the lung microbiome in at-risk individuals.

STAR★METHODS

Detailed methods are provided in the online version of this paper and include the following:

- KEY RESOURCES TABLE
- RESOURCE AVAILABILITY
  - Lead contact
  - Materials availability
  - Data and code availability
- EXPERIMENTAL MODEL AND SUBJECT DETAILS
  - Human subjects
  - Human airway epithelial cells
  - Husbandry and housing conditions of experimental animals
  - Murine intratracheal infection model
  - Ethics approval
- METHOD DETAILS
  - Sputum, serum, and environmental sample collection
  - DNA extraction from clinical and environmental samples
  - Bacterial microbiome sequencing and analysis
  - Microbiological culture of *Neisseria* spp. isolates from the bronchiectasis airway
  - Infection of Air-liquid interface (ALI) cultures with *Neisseria subflava*
  - Trans-epithelial electrical resistance (TEER)
  - Quantification of gene expression by qRT-PCR
  - Immune profiling of mouse bronchoalveolar lavage fluid (BALF)
  - Staining of lung tissue
  - Mouse transcriptome sequencing
  - Metabolite and lipid extraction
  - Instrumental analysis and metabolite-lipid identification

- QUANTIFICATION AND STATISTICAL ANALYSIS
  - Statistical analysis and data visualization
  - Transcriptomic analysis, functional enrichment analysis and weighted correlation network analysis

SUPPLEMENTAL INFORMATION

Supplemental information can be found online at https://doi.org/10.1016/j.chom.2022.08.005.

ACKNOWLEDGMENTS

This research is supported by the Singapore Ministry of Health's National Medical Research Council under its Clinician-Scientist Individual Research Grant (CS-IRG) (MOH-000141) (S.H.C.) and Clinician Scientist Award (CSA) (MOH-000710) (S.H.C.). It is also supported by the National Natural Science Foundation of China (81900071) and the Natural Science Foundation of Guangdong Province of China (2021A1515010004). L.L. is supported by the Research Initiation Fund for Introduction of Talents from the Shenzhen Institute of Advanced Technology, Chinese Academy of Sciences (Y9G077). J.D.C. is supported by a Senior Research Fellowship from the Chief Scientist Office, Scotland (SCAF/17/03) and the British Lung Foundation Chair of Respiratory Research. The authors would like to thank The Academic Respiratory Initiative for Pulmonary Health (TARIPH), Lee Kong Chian School of Medicine, NTU Singapore, for collaboration support.

AUTHOR CONTRIBUTIONS

Study design, S.H.C., J.D.C., M.M.A., L.L., N.S.T., M.F., B.O., P.A.B.W., S.C.S., and W.D.Y.; experiments, L.L., T.X., T.K.J., L.L.Y.C., J.Q., L.W., S.L., K.S.T., and D.I.D.-M.; clinical management of patient cohorts, S.H.C., M.S.K., T.H.O., A.L.Y.H., J.A., T.B.L., T.M.H., J.D.C., A.J.D., H.R.K., and X.L.; data analysis, L.L., M.M.A., T.X., H.S.C., H.R.K., A.J.D., W.D.Y., S.C.S., D.I.D.-M., N.S.T., M.F., J.D.C., and S.H.C.; manuscript, L.L., M.M.A., T.X., T.K.J., L.L.Y.C., L.W., J.Q., N.S.T., M.F., and S.H.C.; all the authors reviewed and agreed to the publication of the study.

DECLARATION OF INTERESTS

J.D.C. has received research grants from GSK, BI, AZ, Gilead Sciences, Grifols, and Insmed and has received personal fees from GSK, BI, AZ, Chiesi, Grifols, Napp, Novartis, Insmed, and Zambon, all outside the submitted work. S.H.C. is on advisory boards for CSL Behring, Pneumagen, and BI, serves on Data and Safety Monitoring Boards for Inovio Pharmaceuticals and Imam Abdulrahman Bin Faisal University, and has received personal fees from AZ, all outside of the submitted work.

Received: December 2, 2021
Revised: May 30, 2022
Accepted: July 18, 2022
Published: September 14, 2022

REFERENCES

Aksamit, T., De Soyza, A., Bandel, T.J., Criollo, M., Elborn, J.S., Operschall, E., Polverino, E., Roth, K., Winthrop, K.L., and Wilson, R. (2018). RESPIRE 2: a phase III placebo-controlled randomised trial of ciprofloxacin dry powder for inhalation in non-cystic fibrosis bronchiectasis. Eur. Respir. J. *51*, 1702053. https://doi.org/10.1183/13993003.02053-2017.

Aliberti, S., Lonni, S., Dore, S., McDonnell, M.J., Goeminne, P.C., Dimakou, K., Fardon, T.C., Rutherford, R., Pesci, A., Restrepo, M.I., et al. (2016). Clinical phenotypes in adult patients with bronchiectasis. Eur. Respir. J. *47*, 1113–1122. https://doi.org/10.1183/13993003.01899-2015.

Bateman, E.D., Hurd, S.S., Barnes, P.J., Bousquet, J., Drazen, J.M., FitzGerald, J.M., Gibson, P., Ohta, K., O'Byrne, P., Pedersen, S.E., et al. (2008). Global strategy for asthma management and prevention: GINA executive summary. Eur. Respir. J. *31*, 143–178. https://doi.org/10.1183/09031936.00138707.

Bronte, V., and Zanovello, P. (2005). Regulation of immune responses by L-arginine metabolism. Nat. Rev. Immunol. *5*, 641–654. https://doi.org/10.1038/nri1668.

Budden, K.F., Shukla, S.D., Rehman, S.F., Bowerman, K.L., Keely, S., Hugenholtz, P., Armstrong-James, D.P.H., Adcock, I.M., Chotirmall, S.H., Chung, K.F., and Hansbro, P.M. (2019). Functional effects of the microbiota in chronic respiratory disease. Lancet Respir. Med. *7*, 907–920. https://doi.org/10.1016/S2213-2600(18)30510-1.

Burkholder, T., Foltz, C., Karlsson, E., Linton, C.G., and Smith, J.M. (2012). Health evaluation of experimental laboratory mice. Curr. Protoc. Mouse Biol. *2*, 145–165. https://doi.org/10.1002/9780470942390.mo110217.

Celli, B.R., and MacNee, W.; ATS/ERS Task Force (2004). Standards for the diagnosis and treatment of patients with COPD: a summary of the ATS/ERS position paper. Eur. Respir. J. *23*, 932–946.

Chalmers, J.D., Chang, A.B., Chotirmall, S.H., Dhar, R., and McShane, P.J. (2018). Bronchiectasis. Nat. Rev. Dis. Primers *4*, 45. https://doi.org/10.1038/s41572-018-0042-3.

Chalmers, J.D., and Chotirmall, S.H. (2018). Bronchiectasis: new therapies and new perspectives. Lancet Respir. Med. *6*, 715–726. https://doi.org/10.1016/S2213-2600(18)30053-5.

Chalmers, J.D., Goeminne, P., Aliberti, S., McDonnell, M.J., Lonni, S., Davidson, J., Poppelwell, L., Salih, W., Pesci, A., Dupont, L.J., et al. (2014). The bronchiectasis severity index. An international derivation and validation study. Am. J. Respir. Crit. Care Med. *189*, 576–585. https://doi.org/10.1164/rccm.201309-1575OC.

Chandrasekaran, R., Mac Aogáin, M., Chalmers, J.D., Elborn, S.J., and Chotirmall, S.H. (2018). Geographic variation in the aetiology, epidemiology and microbiology of bronchiectasis. BMC Pulm. Med. *18*, 83. https://doi.org/10.1186/s12890-018-0638-0.

Chen, S.L., Hoene, M., Li, J., Li, Y.J., Zhao, X.J., Häring, H.U., Schleicher, E.D., Weigert, C., Xu, G.W., and Lehmann, R. (2013). Simultaneous extraction of metabolome and lipidome with methyl tert-butyl ether from a single small tissue sample for ultra-high performance liquid chromatography/mass spectrometry. J. Chromatogr. A *1298*, 9–16. https://doi.org/10.1016/j.chroma.2013.05.019.

Chin, C.S., Alexander, D.H., Marks, P., Klammer, A.A., Drake, J., Heiner, C., Clum, A., Copeland, A., Huddleston, J., Eichler, E.E., et al. (2013). Nonhybrid, finished microbial genome assemblies from long-read SMRT sequencing data. Nat. Methods *10*, 563–569. https://doi.org/10.1038/nmeth.2474.

Chotirmall, S.H. (2018). Future directions: the next 10 years in research. In Bronchiectasis (European Respiratory Society), pp. 371–387.

Chotirmall, S.H., and Chalmers, J.D. (2018). RESPIRE: breathing new life into bronchiectasis. Eur. Respir. J. *51*. https://doi.org/10.1183/13993003.02444-2017.

Chotirmall, S.H., Gellatly, S.L., Budden, K.F., Mac Aogain, M., Shukla, S.D., Wood, D.L., Hugenholtz, P., Pethe, K., and Hansbro, P.M. (2017). Microbiomes in respiratory health and disease: an Asia-Pacific perspective. Respirology *22*, 240–250. https://doi.org/10.1111/resp.12971.

Chotirmall, S.H., O'Donoghue, E., Bennett, K., Gunaratnam, C., O'Neill, S.J., and McElvaney, N.G. (2010). Sputum Candida albicans presages FEV(1) decline and hospital-treated exacerbations in cystic fibrosis. Chest *138*, 1186–1195. https://doi.org/10.1378/chest.09-2996.

Chung, K.F., Wenzel, S.E., Brozek, J.L., Bush, A., Castro, M., Sterk, P.J., Adcock, I.M., Bateman, E.D., Bel, E.H., Bleecker, E.R., et al. (2014). International ERS/ATS guidelines on definition, evaluation and treatment of severe asthma. Eur. Respir. J. *43*, 343–373. https://doi.org/10.1183/09031936.00202013.

Coughlan, C.A., Chotirmall, S.H., Renwick, J., Hassan, T., Low, T.B., Bergsson, G., Eshwika, A., Bennett, K., Dunne, K., Greene, C.M., et al. (2012). The effect of Aspergillus fumigatus infection on vitamin D receptor expression in cystic fibrosis. Am. J. Respir. Crit. Care Med. *186*, 999–1007. https://doi.org/10.1164/rccm.201203-0478OC.

De Soyza, A., Aksamit, T., Bandel, T.J., Criollo, M., Elborn, J.S., Operschall, E., Polverino, E., Roth, K., Winthrop, K.L., and Wilson, R. (2018). RESPIRE 1: a phase III placebo-controlled randomised trial of ciprofloxacin dry powder for inhalation in non-cystic fibrosis bronchiectasis. Eur. Respir. J. *51*, 1702052. https://doi.org/10.1183/13993003.02052-2017.

Dhar, R., Singh, S., Talwar, D., Mohan, M., Tripathi, S.K., Swarnakar, R., Trivedi, S., Rajagopala, S., D'Souza, G., Padmanabhan, A., et al. (2019). Bronchiectasis in India: results from the European Multicentre Bronchiectasis Audit and Research Collaboration (EMBARC) and Respiratory Research Network of India Registry. Lancet Glob. Health *7*, e1269–e1279. https://doi.org/10.1016/S2214-109X(19)30327-4.

Dickson, R.P., Erb-Downward, J.R., Freeman, C.M., McCloskey, L., Falkowski, N.R., Huffnagle, G.B., and Curtis, J.L. (2017). Bacterial topography of the healthy human lower respiratory tract. mBio *8*. e02287–e02216. https://doi.org/10.1128/mBio.02287-16.

Dickson, R.P., Erb-Downward, J.R., and Huffnagle, G.B. (2013). The role of the bacterial microbiome in lung disease. Expert Rev. Respir. Med. *7*, 245–257. https://doi.org/10.1586/ers.13.24.

Domingo-Almenara, X., Montenegro-Burke, J.R., Guijas, C., Majumder, E.L., Benton, H.P., and Siuzdak, G. (2019). Autonomous METLIN-guided in-source fragment annotation for untargeted metabolomics. Anal. Chem. *91*, 3246–3253. https://doi.org/10.1021/acs.analchem.8b03126.

Donati, C., Zolfo, M., Albanese, D., Tin Truong, D., Asnicar, F., Iebba, V., Cavalieri, D., Jousson, O., De Filippo, C., Huttenhower, C., et al. (2016). Uncovering oral Neisseria tropism and persistence using metagenomic sequencing. Nat. Microbiol. *1*, 16070. https://doi.org/10.1038/nmicrobiol.2016.70.

Fanger, N.A., Voigtlaender, D., Liu, C., Swink, S., Wardwell, K., Fisher, J., Graziano, R.F., Pfefferkorn, L.C., and Guyre, P.M. (1997). Characterization of expression, cytokine regulation, and effector function of the high affinity IgG receptor Fc gamma RI (CD64) expressed on human blood dendritic cells. J. Immunol. *158*, 3090–3098.

Finch, S., McDonnell, M.J., Abo-Leyah, H., Aliberti, S., and Chalmers, J.D. (2015). A comprehensive analysis of the impact of Pseudomonas aeruginosa colonization on prognosis in adult bronchiectasis. Ann. Am. Thorac. Soc. *12*, 1602–1611. https://doi.org/10.1513/AnnalsATS.201506-333OC.

Flume, P.A., Chalmers, J.D., and Olivier, K.N. (2018). Advances in bronchiectasis: endotyping, genetics, microbiome, and disease heterogeneity. Lancet *392*, 880–890. https://doi.org/10.1016/S0140-6736(18)31767-7.

Fuschillo, S., De Felice, A., and Balzano, G. (2008). Mucosal inflammation in idiopathic bronchiectasis: cellular and molecular mechanisms. Eur. Respir. J. *31*, 396–406. https://doi.org/10.1183/09031936.00069007.

Gao, B., Gallagher, T., Zhang, Y., Elbadawi-Sidhu, M., Lai, Z., Fiehn, O., and Whiteson, K.L. (2018). Tracking polymicrobial metabolism in cystic fibrosis airways: Pseudomonas aeruginosa metabolism and physiology are influenced by rothia mucilaginosa-derived metabolites. mSphere *3*. e00151–e00118. https://doi.org/10.1128/mSphere.00151-18.

Gaschler, G.J., Skrtic, M., Zavitz, C.C., Lindahl, M., Onnervik, P.O., Murphy, T.F., Sethi, S., and Stämpfli, M.R. (2009). Bacteria challenge in smoke-exposed mice exacerbates inflammation and skews the inflammatory profile. Am. J. Respir. Crit. Care Med. *179*, 666–675. https://doi.org/10.1164/rccm.200808-1306OC.

Global Initiative for Asthma. (2019). Global Management and Prevention. www.ginasthma.org.

GOLD (2018). Global Strategy for the Diagnosis, Management and Prevention of COPD (Global Initiative for Chronic Obstructive Lung Disease). http://goldcopd.org/.

Grassmé, H., Gulbins, E., Brenner, B., Ferlinz, K., Sandhoff, K., Harzer, K., Lang, F., and Meyer, T.F. (1997). Acidic sphingomyelinase mediates entry of N. gonorrhoeae into nonphagocytic cells. Cell *91*, 605–615. https://doi.org/10.1016/S0092-8674(00)80448-1.

Grassmé, H., Jendrossek, V., Riehle, A., von Kürthy, G., Berger, J., Schwarz, H., Weller, M., Kolesnick, R., and Gulbins, E. (2003). Host defense against Pseudomonas aeruginosa requires ceramide-rich membrane rafts. Nat. Med. *9*, 322–330. https://doi.org/10.1038/nm823.

Gregory, L.G., Jones, C.P., Mathie, S.A., Pegorier, S., and Lloyd, C.M. (2013). Endothelin-1 directs airway remodeling and hyper-reactivity in a murine asthma model. Allergy *68*, 1579–1588. https://doi.org/10.1111/all.12271.

Gusareva, E.S., Acerbi, E., Lau, K.J.X., Luhung, I., Premkrishnan, B.N.V., Kolundžija, S., Purbojati, R.W., Wong, A., Houghton, J.N.I., Miller, D., et al. (2019). Microbial communities in the tropical air ecosystem follow a precise diel cycle. Proc. Natl. Acad. Sci. USA *116*, 23299–23308. https://doi.org/10.1073/pnas.1908493116.

Harrell, F.E., Jr. (2019). Package 'Hmisc' (CRAN2018), pp. 235–236. https://cran.r-project.org/web/packages/Hmisc/.

Hill, A.T., Haworth, C.S., Aliberti, S., Barker, A., Blasi, F., Boersma, W., Chalmers, J.D., De Soyza, A., Dimakou, K., Elborn, J.S., et al. (2017). Pulmonary exacerbation in adults with bronchiectasis: a consensus definition for clinical research. Eur. Respir. J. *49*. https://doi.org/10.1183/13993003.00051-2017.

Huson, D.H., Beier, S., Flade, I., Górska, A., El-Hadidi, M., Mitra, S., Ruscheweyh, H.J., and Tappu, R. (2016). MEGAN community edition - interactive exploration and analysis of large-scale microbiome sequencing data. PLoS Comput. Biol. *12*, e1004957. https://doi.org/10.1371/journal.pcbi.1004957.

Ivanisevic, J., Zhu, Z.J., Plate, L., Tautenhahn, R., Chen, S., O'Brien, P.J., Johnson, C.H., Marletta, M.A., Patti, G.J., and Siuzdak, G. (2013). Toward 'omic scale metabolite profiling: a dual separation-mass spectrometry approach for coverage of lipid and central carbon metabolism. Anal. Chem. *85*, 6876–6884. https://doi.org/10.1021/ac401140h.

Kadioglu, A., Gingles, N.A., Grattan, K., Kerr, A., Mitchell, T.J., and Andrew, P.W. (2000). Host cellular immune response to pneumococcal lung infection in mice. Infect. Immun. *68*, 492–501. https://doi.org/10.1128/IAI.68.2.492-501.2000.

King, P.T. (2018). The role of the immune response in the pathogenesis of bronchiectasis. BioMed Res. Int. *2018*, 6802637. https://doi.org/10.1155/2018/6802637.

Kukavica-Ibrulj, I., Facchini, M., Cigana, C., Levesque, R.C., and Bragonzi, A. (2014). Assessing Pseudomonas aeruginosa virulence and the host response using murine models of acute and chronic lung infection. Methods Mol. Biol. *1149*, 757–771. https://doi.org/10.1007/978-1-4939-0473-0_58.

Langfelder, P., and Horvath, S. (2008). WGCNA: an R package for weighted correlation network analysis. BMC Bioinformatics *9*, 559. https://doi.org/10.1186/1471-2105-9-559.

Layeghifard, M., Li, H., Wang, P.W., Donaldson, S.L., Coburn, B., Clark, S.T., Caballero, J.D., Zhang, Y., Tullis, D.E., Yau, Y.C.W., et al. (2019). Microbiome networks and change-point analysis reveal key community changes associated with cystic fibrosis pulmonary exacerbations. NPJ Biofilms Microbiomes *5*, 4. https://doi.org/10.1038/s41522-018-0077-y.

Letunic, I., and Bork, P. (2019). Interactive Tree Of Life (iTOL) v4: recent updates and new developments. Nucleic Acids Res. *47*, W256–W259. https://doi.org/10.1093/nar/gkz239.

Lin, H., and Peddada, S.D. (2020). Analysis of compositions of microbiomes with bias correction. Nat. Commun. *11*, 3514. https://doi.org/10.1038/s41467-020-17041-7.

Liu, G., Tang, C.M., and Exley, R.M. (2015). Non-pathogenic Neisseria: members of an abundant, multi-habitat, diverse genus. Microbiology *161*, 1297–1312. https://doi.org/10.1099/mic.0.000086.

Love, M.I., Huber, W., and Anders, S. (2014). Moderated estimation of fold change and dispersion for RNA-seq data with DESeq2. Genome Biol. *15*, 550. https://doi.org/10.1186/s13059-014-0550-8.

Luhung, I., Uchida, A., Lim, S.B.Y., Gaultier, N.E., Kee, C., Lau, K.J.X., Gusareva, E.S., Heinle, C.E., Wong, A., Premkrishnan, B.N.V., et al. (2021). Experimental parameters defining ultra-low biomass bioaerosol analysis. NPJ Biofilms Microbiomes *7*, 37. https://doi.org/10.1038/s41522-021-00209-4.

Mac Aogáin, M., Lau, K.J.X., Cai, Z., Kumar Narayana, J., Purbojati, R.W., Drautz-Moses, D.I., Gaultier, N.E., Jaggi, T.K., Tiew, P.Y., Ong, T.H., et al. (2020). Metagenomics reveals a core macrolide resistome related to

microbiota in chronic respiratory disease. Am. J. Respir. Crit. Care Med. *202*, 433–447. https://doi.org/10.1164/rccm.201911-2202OC.

Mac Aogáin, M., Narayana, J.K., Tiew, P.Y., Ali, N.A.B.M., Yong, V.F.L., Jaggi, T.K., Lim, A.Y.H., Keir, H.R., Dicker, A.J., Thng, K.X., et al. (2021). Integrative microbiomics in bronchiectasis exacerbations. Nat. Med. *27*, 688–699. https://doi.org/10.1038/s41591-021-01289-7.

Mac Aogáin, M., Tiew, P.Y., Lim, A.Y.H., Low, T.B., Tan, G.L., Hassan, T., Ong, T.H., Pang, S.L., Lee, Z.Y., Gwee, X.W., et al. (2019). Distinct "Immunoallertypes" of disease and high frequencies of sensitization in non-cystic fibrosis bronchiectasis. Am. J. Respir. Crit. Care Med. *199*, 842–853. https://doi.org/10.1164/rccm.201807-1355OC.

Mac Aogáin, M., Chandrasekaran, R., Lim, A.Y.H., Low, T.B., Tan, G.L., Hassan, T., Ong, T.H., Hui Qi Ng, A., Bertrand, D., Koh, J.Y., et al. (2018). Immunological corollary of the pulmonary mycobiome in bronchiectasis: the CAMEB study. Eur. Respir. J. *52*. https://doi.org/10.1183/13993003.00766-2018.

MacDonald, P.L., and Gardner, R.C. (2000). Type I error rate comparisons of post hoc procedures for I j chi-square tables. Educ. Psychol. Meas. *60*, 735–754.

McShane, P.J. (2019). A new bronchiectasis endophenotype: Immunoallertypes. Am. J. Respir. Crit. Care Med. *199*, 811–812. https://doi.org/10.1164/rccm.201810-1949ED.

Menzel, P., Ng, K.L., and Krogh, A. (2016). Fast and sensitive taxonomic classification for metagenomics with Kaiju. Nat. Commun. *7*, 11257. https://doi.org/10.1038/ncomms11257.

Metersky, M., and Chalmers, J. (2019). Bronchiectasis insanity: doing the same thing over and over again and expecting different results? F1000Res. *8*, 8. https://doi.org/10.12688/f1000research.17295.1.

Nearing, J.T., Douglas, G.M., Hayes, M.G., MacDonald, J., Desai, D.K., Allward, N., Jones, C.M.A., Wright, R.J., Dhanani, A.S., Comeau, A.M., and Langille, M.G.I. (2022). Microbiome differential abundance methods produce different results across 38 datasets. Nat. Commun. *13*, 342. https://doi.org/10.1038/s41467-022-28034-z.

O'Dwyer, D.N., Dickson, R.P., and Moore, B.B. (2016). The lung microbiome, immunity, and the pathogenesis of chronic lung disease. J. Immunol. *196*, 4839–4847. https://doi.org/10.4049/jimmunol.1600279.

Oksanen, J., Blanchet, F.G., Kindt, R., Legendre, P., Minchin, P.R., O'Hara, R., Simpson, G.L., Solymos, P., Stevens, M.H.H., and Wagner, H. (2013). Package 'vegan'. Community ecology package, version 2.

Ong, S.H., Kukkillaya, V.U., Wilm, A., Lay, C., Ho, E.X., Low, L., Hibberd, M.L., and Nagarajan, N. (2013). Species identification and profiling of complex microbial communities using shotgun Illumina sequencing of 16S rRNA amplicon sequences. PLoS One *8*, e60811. https://doi.org/10.1371/journal.pone.0060811.

Ovstebø, R., Olstad, O.K., Brusletto, B., Møller, A.S., Aase, A., Haug, K.B., Brandtzaeg, P., and Kierulf, P. (2008). Identification of genes particularly sensitive to lipopolysaccharide (LPS) in human monocytes induced by wild-type versus LPS-deficient Neisseria meningitidis strains. Infect. Immun. *76*, 2685–2695. https://doi.org/10.1128/IAI.01625-07.

Page, A.J., Cummins, C.A., Hunt, M., Wong, V.K., Reuter, S., Holden, M.T., Fookes, M., Falush, D., Keane, J.A., and Parkhill, J. (2015). Roary: rapid large-scale prokaryote pan genome analysis. Bioinformatics *31*, 3691–3693. https://doi.org/10.1093/bioinformatics/btv421.

Pasteur, M.C., Bilton, D., and Hill, A.T.; British Thoracic Society Bronchiectasis non-CF Guideline Group (2010). British Thoracic Society guideline for non-CF bronchiectasis. Thorax *65*, i1–i58. https://doi.org/10.1136/thx.2010.136119.

Pellegrino, R., Viegi, G., Brusasco, V., Crapo, R.O., Burgos, F., Casaburi, R., Coates, A., van der Grinten, C.P., Gustafsson, P., Hankinson, J., et al. (2005). Interpretative strategies for lung function tests. Eur. Respir. J. *26*, 948–968. https://doi.org/10.1183/09031936.05.00035205.

Reimand, J., Isserlin, R., Voisin, V., Kucera, M., Tannus-Lopes, C., Rostamianfar, A., Wadi, L., Meyer, M., Wong, J., Xu, C., et al. (2019). Pathway enrichment analysis and visualization of omics data using g:profiler, GSEA, cytoscape and EnrichmentMap. Nat. Protoc. *14*, 482–517. https://doi.org/10.1038/s41596-018-0103-9.

Richardson, H., Dicker, A.J., Barclay, H., and Chalmers, J.D. (2019). The microbiome in bronchiectasis. Eur. Respir. Rev. *28*, 190048. https://doi.org/10.1183/16000617.0048-2019.

Rigauts, C., Aizawa, J., Taylor, S.L., Rogers, G.B., Govaerts, M., Cos, P., Ostyn, L., Sims, S., Vandeplassche, E., Sze, M., et al. (2022). Rothia mucilaginosa is an anti-inflammatory bacterium in the respiratory tract of patients with chronic lung disease. Eur. Respir. J. *59*, 2101293. https://doi.org/10.1183/13993003.01293-2021.

Rogers, G.B., Bruce, K.D., Martin, M.L., Burr, L.D., and Serisier, D.J. (2014a). The effect of long-term macrolide treatment on respiratory microbiota composition in non-cystic fibrosis bronchiectasis: an analysis from the randomised, double-blind, placebo-controlled BLESS trial. Lancet Respir. Med. *2*, 988–996. https://doi.org/10.1016/S2213-2600(14)70213-9.

Rogers, G.B., Zain, N.M., Bruce, K.D., Burr, L.D., Chen, A.C., Rivett, D.W., McGuckin, M.A., and Serisier, D.J. (2014b). A novel microbiota stratification system predicts future exacerbations in bronchiectasis. Ann. Am. Thorac. Soc. *11*, 496–503. https://doi.org/10.1513/AnnalsATS.201310-335OC.

Schmidt, R., Meier, U., Yabut-Perez, M., Walmrath, D., Grimminger, F., Seeger, W., and Günther, A. (2001). Alteration of fatty acid profiles in different pulmonary surfactant phospholipids in acute respiratory distress syndrome and severe pneumonia. Am. J. Respir. Crit. Care Med. *163*, 95–100. https://doi.org/10.1164/ajrccm.163.1.9903029.

Segal, L.N., Clemente, J.C., Tsay, J.C., Koralov, S.B., Keller, B.C., Wu, B.G., Li, Y., Shen, N., Ghedin, E., Morris, A., et al. (2016). Enrichment of the lung microbiome with oral taxa is associated with lung inflammation of a Th17 phenotype. Nat. Microbiol. *1*, 16031. https://doi.org/10.1038/nmicrobiol.2016.31.

Segata, N., Izard, J., Waldron, L., Gevers, D., Miropolsky, L., Garrett, W.S., and Huttenhower, C. (2011). Metagenomic biomarker discovery and explanation. Genome Biol. *12*, R60.

Smith, C.A., Want, E.J., O'Maille, G., Abagyan, R., and Siuzdak, G. (2006). XCMS: processing mass spectrometry data for metabolite profiling using nonlinear peak alignment, matching, and identification. Anal. Chem. *78*, 779–787. https://doi.org/10.1021/ac051437y.

Sud, M., Fahy, E., Cotter, D., Brown, A., Dennis, E.A., Glass, C.K., Merrill, A.H., Jr., Murphy, R.C., Raetz, C.R., Russell, D.W., and Subramaniam, S. (2007). LMSD: LIPID MAPS structure database. Nucleic Acids Res. *35*, D527–D532. https://doi.org/10.1093/nar/gkl838.

Sutherland, T.C., Quattroni, P., Exley, R.M., and Tang, C.M. (2010). Transcellular passage of Neisseria meningitidis across a polarized respiratory epithelium. Infect. Immun. *78*, 3832–3847. https://doi.org/10.1128/IAI.01377-09.

Taylor, S.L., Rogers, G.B., Chen, A.C., Burr, L.D., McGuckin, M.A., and Serisier, D.J. (2015). Matrix metalloproteinases vary with airway microbiota composition and lung function in non-cystic fibrosis bronchiectasis. Ann. Am. Thorac. Soc. *12*, 701–707. https://doi.org/10.1513/AnnalsATS.201411-513OC.

Tiew, P.Y., Ko, F.W.S., Pang, S.L., Matta, S.A., Sio, Y.Y., Poh, M.E., Lau, K.J.X., Mac Aogáin, M., Jaggi, T.K., Ivan, F.X., et al. (2020). Environmental fungal sensitisation associates with poorer clinical outcomes in COPD. Eur. Respir. J. *56*, 2000418. https://doi.org/10.1183/13993003.00418-2020.

Tsugawa, H., Cajka, T., Kind, T., Ma, Y., Higgins, B., Ikeda, K., Kanazawa, M., VanderGheynst, J., Fiehn, O., and Arita, M. (2015). MS-DIAL: data-independent MS/MS deconvolution for comprehensive metabolome analysis. Nat. Methods *12*, 523–526. https://doi.org/10.1038/nmeth.3393.

Walker, B.J., Abeel, T., Shea, T., Priest, M., Abouelliel, A., Sakthikumar, S., Cuomo, C.A., Zeng, Q., Wortman, J., Young, S.K., et al. (2014). Pilon: an integrated tool for comprehensive microbial variant detection and genome assembly improvement. PLoS One *9*, e112963. https://doi.org/10.1371/journal.pone.0112963.

Wenzel, S.E. (1997). Arachidonic acid metabolites: mediators of inflammation in asthma. Pharmacotherapy *17*, 3S–12S.

Weyand, N.J. (2017). Neisseria models of infection and persistence in the upper respiratory tract. Pathog. Dis. *75*, 1–13. https://doi.org/10.1093/femspd/ftx031.

Wheelock, C.E., Goss, V.M., Balgoma, D., Nicholas, B., Brandsma, J., Skipp, P.J., Snowden, S., Burg, D., D'Amico, A., Horvath, I., et al. (2013). Application of 'omics technologies to biomarker discovery in inflammatory lung diseases. Eur. Respir. J. *42*, 802–825. https://doi.org/10.1183/09031936.00078812.

Whelan, F.J., Waddell, B., Syed, S.A., Shekarriz, S., Rabin, H.R., Parkins, M.D., and Surette, M.G. (2020). Culture-enriched metagenomic sequencing enables in-depth profiling of the cystic fibrosis lung microbiota. Nat. Microbiol. *5*, 379–390. https://doi.org/10.1038/s41564-019-0643-y.

Wickham, H. (2016). ggplot2: elegant graphics for data analysis (Springer).

Wu, B.G., Sulaiman, I., Tsay, J.J., Perez, L., Franca, B., Li, Y., Wang, J., Gonzalez, A.N., El-Ashmawy, M., Carpenito, J., et al. (2021). Episodic aspiration with oral commensals induces a MyD88-dependent, pulmonary T-helper cell Type 17 response that mitigates susceptibility to Streptococcus pneumoniae. Am. J. Respir. Crit. Care Med. *203*, 1099–1111. https://doi.org/10.1164/rccm.202005-1596OC.

Xu, T., Lim, Y.T., Chen, L., Zhao, H., Low, J.H., Xia, Y., Sobota, R.M., and Fang, M. (2020). A novel mechanism of Monoethylhexyl phthalate in lipid accumulation via inhibiting fatty acid beta-oxidation on hepatic cells. Environ. Sci. Technol. *54*, 15925–15934. https://doi.org/10.1021/acs.est.0c01073.

You, D., Becnel, D., Wang, K., Ripple, M., Daly, M., and Cormier, S.A. (2006). Exposure of neonates to respiratory syncytial virus is critical in determining subsequent airway response in adults. Respir. Res. *7*, 107. https://doi.org/10.1186/1465-9921-7-107.

STAR★METHODS

KEY RESOURCES TABLE

REAGENT or RESOURCE	SOURCE	IDENTIFIER
Antibodies		
PE anti-mouse CD45 Antibody Clone 30-F11	Biolegend	RRID:AB_312971
APC/Cyanine7 anti-mouse CD45 Antibody clone 30-F11	Biolegend	RRID:AB_312981
APC anti-mouse Ly-6G Antibody Clone 1A8	Biolegend	RRID:AB_2227348
Anti-F4/80 antibody [BM8] (FITC)	Abcam	RRID:AB_941505
APC anti-mouse NK-1.1 Antibody clone PK136	Biolegend	RRID:AB_313397
FITC anti-mouse CD19 antibody clone 6D5	Biolegend	RRID:AB_313641
Ms CD3 Molecular Complex FITC 17A2	BD Biosciences	RRID:AB_2920870
PE anti-mouse CD4 Antibody Clone H129.19	Biolegend	RRID:AB_2075573
APC anti-mouse CD8a Antibody Clone 53-6.7	Biolegend	RRID:AB_312751
Bacterial and virus strains		
Clinical respiratory isolates of *Neisseria subflava*.	Singapore General Hospital, Tan Tock Seng Hospital, Changi General Hospital, Singapore.	N/A
Biological samples		
Sputum and serum samples from bronchiectasis patients (Singapore)	Singapore General Hospital, Tan Tock Seng Hospital, Changi General Hospital, Singapore.	N/A
Sputum samples from bronchiectasis patients (Malaysia)	UKM Medical Centre, Kuala Lumpur, Malaysia	N/A
Sputum samples from bronchiectasis patients (Dundee)	Ninewells Hospital and Medical School, Dundee, Scotland, United Kingdom	N/A
Sputum samples from COPD patients (Singapore)	Singapore General Hospital, Singapore.	N/A
Sputum samples from Severe Asthma patients (Singapore)	Singapore General Hospital, Singapore.	N/A
Sputum samples from COPD patients (Dundee)	Ninewells Hospital and Medical School, Dundee, Scotland, United Kingdom	N/A
Sputum samples from Severe Asthma patients (Dundee)	Ninewells Hospital and Medical School, Dundee, Scotland, United Kingdom	N/A
Sputum and serum samples from healthy controls (Singapore)	Nanyang Technological University, Singapore.	N/A
Lung biopsy samples from bronchiectasis patients and controls	Department of Respiratory Medicine and Critical Care, Peking University Shenzhen Hospital.	N/A
Chemicals, peptides, and recombinant proteins		
Sputasol	Thermo Fisher	SR0233A
RNALater	Thermo Fisher	AM7021
Giemsa Staining Solution	Beyotime	C0133
DAPI	Beyotime	C1006
TRIzol	Thermo Fisher	15596026
Critical commercial assays		
Hematoxylin and Eosin Staining Kit	Beyotime	C0105M

(*Continued on next page*)

Continued

REAGENT or RESOURCE	SOURCE	IDENTIFIER
High Pure PCR Template Preparation Kit	Roche diagnostics	11796828001
Deposited data		
16S amplicon sequencing data	NCBI	BioProject: PRJNA590225
Whole genome sequence assemblies of *Neisseria subflava* clinical respiratory isolates	NCBI	BioProject: PRJNA714914
RNA sequencing data of the *Neisseria subflava* infection model	NCBI	BioProject: PRJNA706545
Metabolomics and lipidomics datasets from the *Neisseria subflava* infection model	EMBL-EBI	MetaboLights: MTBLS3009
Metagenomic sequencing data	NCBI	BioProject: PRJNA595703
Experimental models: Cell lines		
Human nasopharyngeal epithelial cells	Singapore General Hospital and National University Hospital, Singapore, John Hunter Hospital, NSW, Australia	N/A
Human bronchial epithelial cells	John Hunter Hospital, NSW, Australia	N/A
Experimental models: Organisms/strains		
Mouse: C57BL/6J	Jackson Laboratory	000664
Oligonucleotides		
See Table S7 in supplemental information.		
Software and algorithms		
All original code	This manuscript	https://github.com/RespiratoryMicrobiome/Neisseria; https://doi.org/10.5281/zenodo.6969817
CLC Genomics Workbench 9.0	CLC genomics.	N/A
DESeq2	Love et al., 2014	N/A
Ingenuity Pathway Analysis (IPA) software	Qiagen Bioinformatics.	N/A
XCMS	Smith et al., 2006	N/A
R package "Hmisc"	Harrell, 2019	N/A
R package "ggplot2"	Wickham, 2016	N/A
R package "vegan"	Oksanen et al., 2013	N/A
R Package "Weighted correlation network analysis (WGCNA)"	Langfelder and Horvath, 2008	N/A
LEfSe	Segata et al., 2011	N/A
Cytoscape	Reimand et al., 2019	N/A
MEGAN	Huson et al., 2016	N/A

RESOURCE AVAILABILITY

Lead contact

Further information and requests for resources and reagents should be directed to and will be fulfilled by the lead contact, Sanjay H. Chotirmall (schotirmall@ntu.edu.sg).

Materials availability

This study did not generate new unique reagents.

Data and code availability

- All raw sequencing and metabolipidomic data have been deposited in NCBI-SRA and MetaboLights database (EMBL-EBI) respectively. Public accession numbers associated with 16S rRNA gene amplicon sequencing data, mouse transcriptomic RNA sequencing data, metabolomics and lipidomics data, sputum and environmental metagenomic whole genome shotgun (WGS) data and *Neisseria subflava* genome assemblies are described in the key resources table.

- All original code and additional processed data outputs associated with this manuscript have been deposited in GitHub repository https://github.com/RespiratoryMicrobiome/Neisseria (release v1.0.0 https://doi.org/10.5281/zenodo.6969817). Processed data is also presented in Table S3.
- Any additional information required to reanalyze the data reported in this paper is available from the lead contact upon reasonable request and needs to abide by approved ethical and legal policies.

EXPERIMENTAL MODEL AND SUBJECT DETAILS

Human subjects

Four human cohorts were recruited in this study each receiving appropriate ethical approvals (detailed below) from all respective participating centers. All recruited individuals provided written informed consent for participation in this study. The four cohorts are summarized as follows:

(1) A cross-sectional Cohort of Asian and Matched European Bronchiectasis (CAMEB), consisting of individuals with high-resolution computed tomography (HRCT) confirmed bronchiectasis and recruited during outpatient attendance when clinically stable, defined as the absence of new symptoms or change to bronchiectasis therapy in the preceding four-weeks. Patients were recruited from three sites in Singapore (Singapore General Hospital, Changi General Hospital and Tan Tock Seng Hospital), one Malaysian site (UKM Medical Centre, Kuala Lumpur) and an age-, sex- and disease-severity matched group (based on Bronchiectasis Severity Index - BSI) from a single European site (Ninewells Hospital, Dundee, UK) to control for confounding geographic factors (Chalmers et al., 2014; Mac Aogáin et al., 2018). Patients with another concurrent major respiratory disease as their primary diagnosis (i.e., asthma or COPD) (Bateman et al., 2008; Celli et al., 2004), those pregnant or breastfeeding, active mycobacterial disease or on chemotherapy were excluded along with patients with active infection (necessitating acute use of antibiotics) and/or received systemic corticosteroids in the four weeks preceding recruitment. Central to the CAMEB cohort strategy was the 'matching' of individuals recruited from Asia (Singapore and Kuala Lumpur, Malaysia) to an individual from Europe (Dundee, Scotland) to permit geographic comparisons between the cohorts (Chalmers et al., 2014; Mac Aogáin et al., 2018). This current study focused on the assessment of geographic variation in the bacterial microbiome between Asian and European patients from the CAMEB cohort. A total of n=225 patients from the cohort had their sputum assessed, generating 16S rRNA bacteriome profiles. This included n=95 'matched' Asian-European pairs. Further details about the CAMEB cohort, including demographics, recruitment, patient matching, and inclusion and exclusion criteria are described previously (Mac Aogáin et al., 2019; Mac Aogáin et al., 2018, 2021) and demographics for the individuals included in this particular study are summarized in Table S1.

(2) For the assessment of *Neisseria* spp. in the lower airway, a cohort of n=21 individuals from a single center in Peking University Shenzhen Hospital, China was recruited. Lung biopsies were obtained from n=9 individuals with clinically and radiologically confirmed bronchiectasis and n=12 non-bronchiectasis (control) subjects. Patients in the bronchiectasis group had a prior history of bronchiectasis confirmed by clinical and radiological assessment, including computed tomography (CT) of the chest. Control subjects represented individuals undergoing bronchoscopy with a radiological suspicion of lung cancer. All control subjects had no demonstrable radiological evidence of bronchiectasis as defined by established criteria including increased or abnormal bronchiolar diameter or appearance, signet ring sign or thickening of bronchiolar walls (Pasteur et al., 2010). Formalin-fixed paraffin-embedded specimens of lung tissue were obtained in all patients, which for all subjects were taken approximately 2 cm from the carina from within a main bronchi in macroscopically 'normal' appearing regions. Demographics for the individuals included in this cohort are summarized in Table S2.

(3) For whole-genome shotgun (WGS) metagenomics analysis of the airway microbiome in non-diseased (healthy) individuals (n=8) and those with chronic respiratory disease (n=28), a spontaneously expectorated sputum sample was obtained from a deep cough in healthy subjects (n=8, Singapore) and patients with bronchiectasis (n=12; 6 Singapore and 6 Dundee); severe asthma (n=8; 4 Singapore and 4 Dundee) and chronic obstructive pulmonary disease (COPD) (n=8; 4 Singapore and 4 Dundee). Non-diseased (healthy) subjects had no active or past history of any respiratory or other medical disease and had normal spirometry measured in accordance with ERS/ATS criteria (Pellegrino et al., 2005). Severe asthma was defined as an individual attending a dedicated severe asthma service at a tertiary referral center for at least 2 years. Patients were free from exacerbation over the preceding four-week period prior to sampling and were at least at step four of the Global Initiative for Asthma (GINA) treatment ladder (Global Initiative for Asthma, 2019; Chung et al., 2014), while COPD was defined according to the global initiative for chronic obstructive lung disease (GOLD), where FEV1/FVC<0.7, sampled during periods of disease stability defined as the absence of exacerbation over the preceding 6 weeks before study recruitment (GOLD, 2018 [http://goldcopd.org/]; Tiew et al., 2020). The demographics and clinical details of the individuals included in this cohort are summarized in Table S5.

(4) Stable, *Neisseria*-dominant bronchiectasis patients (n=10) were recruited in Singapore for home and environmental sampling. As outlined above, patients had HRCT-confirmed bronchiectasis and were recruited during outpatient attendance during a period of clinical stability, consistent with the CAMEB study protocol. Sampling in this study arm involved collection of 1) an indoor (bedroom) air sample, 2) a concurrently obtained outdoor (balcony) air sample, 3) a surface swab obtained from

either an air-conditioning filter or fan within the individual bedroom in addition to 4) a surface swab of the patient inhaler device and 5) an individual sputum sample. Demographics for the individuals included in the home sampling part of the study are summarized in Table S6.

For validation of metabolipidomic experiments, serum samples from six *Neisseria*-dominant and six *Pseudomonas*-dominant patients from Asia and the CAMEB cohort, in addition to six healthy controls were compared (Table S4).

For demographic reporting and the presented analysis, bronchiectasis disease severity was assigned according to the multimodal Bronchiectasis Severity Index (BSI) and further divided into 'mild' (BSI; 0-4), 'moderate' (BSI; 5-8) or 'severe' (BSI; 9 and above) categories. Clinical data comprising the BSI including age, body mass index (BMI), Medical Research Council (MRC) dyspnea score, FEV1 percentage predicted values, radiological severity, number of exacerbations (defined by BTS consensus criteria) in the preceding year, hospitalizations in the preceding year, microbial colonization with other organisms and colonization by *P. aeruginosa* were recorded for each patient, including data on sex, disease etiology and smoking status (Chalmers et al., 2014; Hill et al., 2017).

Individuals recruited into this study were either healthy (with normal immune status) or diagnosed with a chronic respiratory disease (as described above). In this latter group, relative functional immunodeficiencies related to underlying disease pathogenesis may be present however unless otherwise stated, none had any formal diagnosis of a primary or secondary immunodeficiency syndrome.

Human airway epithelial cells

Nasopharyngeal and bronchial sampling respectively were performed according to established protocols by trained personnel using flocked nasopharyngeal swabs (FNPS) with the BBL Universal Viral Transport Standard Kit or obtained using a single sheathed nylon cytology brush applied under direct vision during bronchoscopy. For nasopharyngeal sampling, a FNPS was inserted into the nostril to an appropriate depth and rotated several times before removal. For bronchial sampling, approximately 4-8 brushings were taken from second to third generation bronchi, and cells were washed from brushes with DMEM. Samples were immediately transferred on ice to the laboratory for further processing as described. *Human nasopharyngeal epithelial cells (HNECs)*: Flocked nasopharyngeal swabs (FNPS) were flushed with transport medium at least 20 times to release HNECs. Cells were plated on human collagen IV precoated 6-well plates and cultured in B/D expansion medium (1:1 advanced DMEM/F12 and Bronchial epithelial cell medium (BEPICM) supplemented with 1x BEpiCGS, 1% of HEPES, 1% of Glutamax, 1x B27, penicillin/streptomycin (100 μg/ml), primocin (50 μg/ml), R-spondin 1 (500 ng/ml) epinephrine (0.5 μg/ml), N-acetyl-cysteine (1.25 mM), nicotinamide (5 mM), Y-27632 (5 μM), DMH-1 (1 μM), 3,3',5-triido-L-thyronine (100 nM), SB202190 (500 nM), A83-01 (1 μM), FGF-7 (25 ng/ml), FGF-10 (100 ng/ml) and N-[N-(3,5-difluorophenacetyl)-L-alanyl]-S-phenylglycine t-butyl ester (DAPT) (5 μM)). Medium was refreshed every two days until confluent. *Human bronchial epithelial cells (HBECs)*: Cells were washed with HBSS and plated in a tissue-culture flask in bronchial epithelial growth medium (BEGM) (Lonza, USA) with growth supplements. Medium was refreshed every two days until confluent.

Husbandry and housing conditions of experimental animals

For intratracheal mouse infection experiments, 6- to 10-week old C57BL/6 mice were obtained (Jackson laboratories) and maintained in specific Pathogen Free (SPF) facilities on a 12-hour light-dark cycle with *ad libitum* access to chow and water, in biosafety level 2 (BSL-2) conditions, until experimental inoculation.

Murine intratracheal infection model

At the time of inoculation, mice were anesthetized using 80 mg/kg body weight ketamine and 10 mg/kg body weight xylazine and infected via intratracheal delivery with the cultured *Neisseria subflava* (isolate SG-KL01) at 2 x 10^7 CFU or *Pseudomonas aeruginosa* (strain PAO1) at 1 x 10^6 CFU in 40 μL of sterile phosphate-buffered saline (PBS) once. Mice were monitored for body weight and clinical score (Burkholder et al., 2012). Phenotypic scoring was performed based on indicators of general well-being such as coat condition, normal posture, eyes, and body stance. Mice were scored as follows; '100' - normal posture and shining fur; spontaneous and normal behavior and social contact, clear and clean eyes; normal breathing; '80' - minor symptoms of ruffled fur, spontaneous but reduced behavior, altered breathing; '60' - loss of body weight, moderately reduced activity, ruffled fur, hunched posture, accelerated breathing; '40' - loss of body weight, ruffled fur, motility only after stimulation, massively hunched posture, unclean and sticky, closed or squinted eyes, strongly accelerated breathing; '20' - moribund, '0' - death. Mice were euthanized at specified time points, and lung tissue was harvested. Lung lobes were either fixed in 4% paraformaldehyde for histological analysis or snap-frozen in liquid nitrogen and kept at -80°C for subsequent assays.

Ethics approval

All human cohorts recruited for this study are described as relevant. Participants were recruited from several hospitals and/or academic sites from 5 countries (Singapore, Malaysia, Scotland, China, and Australia) as described in the methods and recruitment approved by their respective institutional review boards as follows. All included participants provided written informed consent: CIRB 2016/2073, UKMMC FF-2016-440, NHD 12/ES/0059, BDSYLSY-053A (bronchiectasis) CIRB 2016/2628, 16/NW/0101 (severe asthma), CIRB 2016/2715, CIRB 2016/2549, 16/NW/0101 (COPD), CIRB 2017/2109 (Home sampling) (all mutually recognized by DSRB), NTU IRB-2017-12-010 (Healthy individuals). HBECs were obtained from the John Hunter Hospital, Australia (H-163-1205, The Hunter New England LHD ethics committee, Australia), and HNECs from CIRB 2020/2338 (Singapore), IRB-2020-05-004 (Nanyang Technological University, Singapore) and NUS under IRB L13-509 and DSRB 2011/00228. All animal experiments were

approved by the Institutional Animal Care and Use Committee (IACUC) at Nanyang Technological University (A18089) and Xiamen University, China (XMULAC20190029).

METHOD DETAILS

Sputum, serum, and environmental sample collection

Spontaneously expectorated 'representative' sputum from a deep cough with the assistance of a chest physiotherapist or induction protocol (where appropriate) was collected into sterile containers and transported (on ice) for evaluation (Chotirmall et al., 2010). All specimens from clinical sites were transported promptly, appropriately and processed centrally at a single site to ensure consistency and standardization of all experimental work and downstream analysis. Samples from the Singaporean hospitals were transported on ice by courier to Nanyang Technological University (within 4 hours of collection). To ensure quality control of materials transported from sites outside Singapore, specimens were shipped on dry ice in temperature-controlled containers and their integrity checked on arrival before experimental use. Equal volumes of Sputasol (Thermo Fisher Scientific) and sputum samples were combined and shaken for 15 minutes at 37°C. Sputasol-homogenized samples were mixed with two volumes of RNAlater (Sigma Aldrich) (Coughlan et al., 2012; Mac Aogáin et al., 2018). Treated sputum samples were sorted at −80°C prior to processing. DNA extraction experiments were performed at Nanyang Technological University, Singapore using a single standardized protocol (outlined in detail below) (Mac Aogáin et al., 2018). Serum was collected from bronchiectasis patients whose sputum microbiome profile was either *Neisseria*- or *Pseudomonas*-dominant in composition, as well as from healthy control subjects (Table S4). To obtain serum, blood specimens were collected in vacutainer serum tubes (BD Biosciences) and centrifuged at 1300 g for 10 minutes at 18°C to separate serum which was subsequently used for the described studies. In addition to sputum and serum, environmental air samples were collected from patient homes using filter-based air samplers SASS3100 (Research International) with a lowered flow rate of 100 L·min−1 (to avoid sleep disruption) for eight consecutive hours. Samplers were placed in the patient's bedroom and near an outdoor air source (i.e., balcony) and programmed to run concurrently overnight at the same time each evening (8pm – 4am). In addition, surface swabs (either air-conditioner or fan where applicable) were taken from the patients' homes: the surfaces of air-conditioning filters or fans in the bedroom and inhaler devices were swabbed using 4N6Floq (Copan) swabs pre-moistened with 0.1% PBS-Triton-X100 and snapped into DNeasy PowerWater kit (Qiagen) bead tubes directly after use. Air filters from SASS samplers were transferred to filter pouches and transported with swabs in bead tubes to the lab for immediate processing or stored at −20°C prior to processing (Gusareva et al., 2019; Mac Aogáin et al., 2020).

DNA extraction from clinical and environmental samples

Sputum DNA was extracted from a 250 mg sample using methods previously described (Coughlan et al., 2012; Mac Aogáin et al., 2018). Stored sputum samples were thawed on ice and transferred to sterile bead mill tubes (VWR) containing 1mm sterile glass beads (Sigma-Aldrich). Samples were homogenised using a bead mill homogeniser (VWR) and DNA was purified using the Roche High-pure PCR Template Preparation Kit (Roche) according to manufacturers' instructions. The integrity of extracted sputum DNA was confirmed using the Qubit dsDNA High Sensitivity (HS) Assay Kit (Invitrogen,). Swab samples in DNeasy PowerWater kit (Qiagen, Germany) bead tubes were processed according to the manufacturer's protocol with the addition of proteinase K (Sigma-Aldrich, USA) and sonication at 65°C (Mac Aogáin et al., 2020). For processing, the SASS filter was transferred to a sterile tube and washed with PBS-Triton X-100 in triplicate. Washed solutions from SASS air filters were further processed by filtering through 0.02 μm Anodisc filters (Whatman) using a vacuum manifold (DHI). DNA was then extracted from the Anodisc with the DNeasy PowerWater kit (Qiagen) according to the manufacturer's protocol with modifications to increase DNA yield (Luhung et al., 2021). Sterile swabs, filters and sputum DNA extraction reagents were processed simultaneously as extraction controls to assess the levels of experimental background contamination (Figure S3).

Bacterial microbiome sequencing and analysis

Targeted amplicon sequencing of the 16S rRNA gene (bacteriome) was carried out on DNA extracted from individuals with bronchiectasis recruited from the CAMEB cohort using a previously validated amplicon shotgun sequencing protocol with paired-end analysis (2 x 101 bp reads) on an Illumina HiSeq2500 platform (Mac Aogáin et al., 2021; Ong et al., 2013). Blank samples were subjected to 16S rRNA analysis capturing and allowing adjustment for background levels of experimental contamination, as shown in Figure S3. Low DNA yield from blanks necessitated pooling (n=4) to ensure sufficient material for amplification and sequencing. The concentration of 16S rRNA amplicons was assessed using Agilent 2100 Bioanalyzer (Agilent Technologies). The amplicon concentrations and read counts observed (as a proxy for bacterial contamination/burden) in test samples and extraction blanks were assessed. Blank samples exhibited considerably lower amplicon concentrations and read counts than those of test samples and therefore background contamination is unlikely to have had a substantial influence on the observed microbiome profiles. Read counts in blanks as well as their taxonomic assignments are illustrated in Figure S3. All 16S rRNA gene short-read sequence data from this study have been uploaded to the National Center for Biotechnology Information (NCBI) sequence read archives under project accession number PRJNA590225. Metagenomic sequencing of sputum and environmental samples was sequenced on a HiSeq 2500 platform (Illumina, USA) at the NTU core sequencing facility according to library preparation and DNA sequencing methods as described (Mac Aogáin et al., 2020, 2021). Read counts in sequencing blank controls for metagenomic analysis as well as their taxonomic assignments are illustrated in Figure S3. The metagenomics sequence data were processed for adaptor removal and quality trimming with a Phred

quality score threshold of 20 (Q<20) using Cutadapt v. 1.8.1. The trimmed reads were then aligned against the NCBI non-redundant protein database using the taxonomic classifier Kaiju (v.1.7.2) (Menzel et al., 2016). Kaiju outputs were imported into MEGAN (v. 5.11.3) (Huson et al., 2016), which uses lowest common ancestry (LCA) algorithm to assign taxon IDs to metagenomic reads based on NCBI taxonomy. The minimum number of reads required for taxonomic assignment was set to 25. Short-read metagenomic sequencing data from this study have been uploaded to the National Center for Biotechnology Information (NCBI) sequence read archives under project accession number PRJNA595703.

Microbiological culture of *Neisseria* spp. isolates from the bronchiectasis airway

The presence of viable *Neisseria* spp. in the sputum of Asian bronchiectasis patients was assessed by inoculation of chocolate agar (BD-BBL) with a loopful of sputum incubated overnight at 37°C under 5% CO_2. Colourless colonies isolated on chocolate agar were presumptively identified by Gram staining, oxidase test and BD BBL™ Crystal™ microbial ID strips (N/H), and further assessed using a commercial MALDI TOF bacterial identification system (Bruker MALDI Biotyper Identification system). Using pure cultures of presumptively identified *Neisseria* spp., high quality genomic DNA was extracted with the Wizard® Genomic DNA Purification Kit for use in more definite confirmation by whole-genome sequence analysis. DNA was further purified by the phenol/chloroform method. DNA was quantified by both nanodrop and qubit quantification. For 10-20kb SMRTbell libraries, the g-DNA concentration was maintained at least at 200ng/ul. Libraries for long-read sequencing were constructed using the SMRTbell Template Prep Kit 1.0 (Pacific Biosciences, USA) and subjected to SMRT sequencing (Pacific Biosciences RSII). Short reads (2x250 bp paired end) were also generated on a MiSeq platform (Illumina) using the NexteraXT library preparation kit (Illumina). De novo assembly of PacBio sequence reads was performed using the Hierarchical Genome Assembly Process (HGAP) version 3 included in the PacBio SMRT Analysis 2.3.0 package (Chin et al., 2013). The assembly was then error corrected and polished with paired end reads from an Illumina MiSeq run using Quiver and Pilon version 1.16, respectively (Walker et al., 2014). Phylogenetic comparison of polished genome assemblies with publicly available reference genomes for several *Neisseria* species, based on core genome alignment, was performed using the Roary pan-genome analysis pipeline with tree visualisation in iTol (Letunic and Bork, 2019; Page et al., 2015). Genome assemblies have been deposited at the National Center for Biotechnology Information (NCBI) under whole genome shotgun (WGS) project accession PRJNA714914.

Infection of Air-liquid interface (ALI) cultures with *Neisseria subflava*

HNECs and HBECs cells were grown to confluence as a monolayer from which $2x10^5$ cells seeded on the apical chamber of a 24-well transwell (Corning transwell 3470) pre-coated with human collagen I (Advanced Biomatrix, USA). The transwell with HNECs or HBECs was first cultured in submerged phase. Once the cell layer became intact, the medium on the apical chamber was removed and the cells were cultured at air-liquid interface (ALI) thereafter. Medium was refreshed twice a week and the HNECs and HBECs were differentiated for 21 days using ALI-Diff medium (Advanced DMEM/F12 supplemented with Penicillin/Streptomycin (100 μg/ml), hydrocortisone (0.5 μg/ml), Epinephrine (0.5 μg/ml), 3,3',5-Triido-L-thyronine (100 nM), human EGF (0.5 ng/ml), TTNPB (100 nM) and A83-01 (50 nM)) before infection experiments. ALI-HNECs or HBECs were cultured in antibiotic-free medium one-week before and throughout infection. The *Neisseria subflava* clinical isolate SG-KL01 was cultured on chocolate agar plate at 37°C under 5% CO2 for 24h. Colonies were picked and dispersed in PBS and gently bead-beaten to yield a homogenous solution. Twenty microlitres of homogenous bacterial suspension at a concentration of at least ~$8.7x\ 10^7$ CFU/ml was added to the apical chamber for infection and incubated at 37°C, 5% CO_2 for 2h. For gene expression experiments, cells were lysed with buffer RLT Plus (Qiagen, USA) with β-mercaptoethanol at 2, 24, 48 and 72 hours post infection (hpi). To quantify internalized bacteria, infected cells were washed twice with PBS both apically and basolaterally to remove external bacteria at 24, 48 and 72 hpi. The cells were refreshed with ALI-Diff medium with 1% penicillin/streptomycin and incubated at 37°C, 5% CO_2 for 1h to kill all the adhered and external bacteria. 0.5% of Triton X-100 was added to the cells for 15 mins at room temperature to detach cells and release the internalized bacteria. Serial dilution of bacterial suspensions was performed and spread-plated on LB agar plates. Plates were incubated at 37°C, 5% CO_2 for 24h to determine CFU/ml.

Trans-epithelial electrical resistance (TEER)

Cellular junction integrity of ALI cultures was assessed before and during infection by measuring the TEER using EVOM2 with STX2 chopstick electrode (World Precision Instruments, USA). TEER values were indicated as $\Omega*cm^2$ and calculated as TEER = (measured value – background value) *surface area of transwell insert in cm^2.

Quantification of gene expression by qRT-PCR

Total RNA was extracted from cell lysates using a Qiagen RNeasy Plus mini kit following manufacturer's instructions. Extracted RNA was then reverse transcribed into cDNA with a PrimeScript RT reagent kit (Takara, Japan). mRNA expression was measured by real-time PCR amplification with GoTaq® qPCR Master Mix (Promega, USA) with specific primers (see Table S7) using an ABI StepOnePlus™ Real-Time PCR System (Applied Biosystems, USA).

Immune profiling of mouse bronchoalveolar lavage fluid (BALF)

Immune cells were harvested from infected mice by bronchoalveolar lavage (BAL). One millilitre of sterile PBS was injected into the mouse lung through the trachea and retrieved into a syringe. BALF contains immune cells and debris from damaged lung tissue. Cells

were pelleted by centrifugation at 500 × g for 10 min and stained by Giemsa (Beyotime) or subjected to flow cytometry. Flow cytometry was performed using a BD FACSAria. The following surface markers were used: macrophages (F4/80-fluorescein isothiocyanate [FITC] and CD45-phycorerythrin [PE]), neutrophils (Ly6G-FITC), natural killer cells (NK1.1-PE), T cytotoxic cells (CD3-allophycocyanin [APC] and CD8-FITC), T-helper cells (CD3-APC and CD4-PE), and B cells (CD19-APC). Unstained cells served as negative controls. Antibodies for cell staining are listed and further detailed in the key resources table.

Staining of lung tissue

Lung tissue samples from either mouse experiments or human biopsies were dehydrated and embedded in paraffin. Five-micrometre sections were next mounted on slides coated with Superfrost Plus (Thermal Scientific). Sections were dewaxed with xylene and rehydrated in water. Hematoxylin and eosin (H&E) staining (Beyotime) was performed for histopathological analysis of lung tissues. The presence of *N. subflava* in lung sections was assessed by employing fluorescent in situ hybridization (FISH) (Fanger et al., 1997). Briefly, following dehydration of fixed lung sections in an ethanol series (3 min each in 50, 80, and 98% ethanol), overnight hybridization to 16S rRNA of *N. subflava* was performed with a probe tagged with Cy5 in a hybridization buffer containing 30% formamide. After washing steps, sections were mounted with an antifade reagent containing DAPI (4',6-diamidino-2-phenylindole, Beyotime), and images captured using an Observer Z1 fluorescence microscope (Carl Zeiss).

Mouse transcriptome sequencing

Murine lung tissue specimens were harvested employing a double-blinded experimental design and involving three independent operators. Samples at each timepoint were harvested in parallel across the experimental conditions and processed promptly (within 2 hours), thus limiting both potential operator-specific and temporal processing effects. Total RNA was extracted from frozen mouse lung tissues using TRIzol (Thermo Fisher). The integrity of the total RNA and level of DNA contamination was assessed using an Agilent 2100 bioanalyzer (Agilent Technologies) and Qubit 2.0 fluorometer (Invitrogen). Library preparation was performed according to the mRNA-seq sample preparation kit (Illumina) and RNA sequencing performed on an Illumina MiSeq platform with single-end 75-bp sequencing. Sequencing reads were mapped to the mouse genome using the CLC Genomics Workbench 9.0. Differential gene expression was determined using the R statistics package DESeq2. The following criteria were adopted to filter the unique sequence reads: maximum number of hits for a read of 1, minimum length fraction of 0.9, minimum similarity fraction of 0.8, and maximum number of two mismatches. A constant of 1 was added to the raw transcript count value to avoid any issues with zero values. Transcript counts were normalized to the effective library size. The differentially expressed genes were identified by performing a negative binomial test and transcripts determined as differentially expressed when they showed a >=2-fold change with an adjusted P value of at least 0.05. Pathway analysis and data presentation was performed using Ingenuity Pathway Analysis (IPA) software (Qiagen Bioinformatics). RNA sequencing data of the *Neisseria subflava* infection model has been deposited in NCBI's Sequence Read Archive (SRA) database under the Accession Number PRJNA706545.

Metabolite and lipid extraction

Lung tissue or serum metabolite (Ivanisevic et al., 2013) and lipid (Chen et al., 2013; Xu et al., 2020) extraction methods were obtained from prior studies. For the lung tissue samples, weighted (~10 mg) freeze-tissue samples were homogenized using steel beads with thaw twice. The suspension was then further split into two portions of 1,000 μL and 200 μL, to be used for metabolomics and lipidomics analysis, respectively. The metabolomic portion was placed at -20°C for 1h, centrifuged at 14,000 rmp/min at 4°C for 20 mins, followed by drying of the supernatant by speed-vacuum evaporator at 4°C. Next, this was dissolved with a weight-normalized volume (10 mg lung tissue equals 100 μL) of ice-cold acetonitrile:H_2O (1:1, v/v) for further mass spectrometry analysis. The 200 μL lipidomics portion was added to methyl tert-butyl ether (MTBE) and water and kept at final ratio of 20:6:7 (MTBE: methanol: H_2O v/v/v) in a glass-vial, followed by sonication (40 kHz and 100 W) for 30 mins in an ice bath, with centrifugation at 3,000 rmp/min at 4°C for 15 mins to facilitate phase separation. The upper organic phase (with enriched lipids) was collected and dried under nitrogen blow, and reconstituted with weight-normalized volume (10 mg lung tissue equals 50 μL) of isopropanol:chloroform:methanol (1:1:1, v/v/v) which was further diluted with same volume of the initial LC-phases for further mass spectrometry analysis. For serum metabolite extraction, both mouse and human samples (Table S4) were used. Here, 400μL ice-cold methanol:acetonitrile (1:1, v/v) was added to 100μL serum, vortexed for 30s, and placed at -20°C for 1h, followed by centrifugation at 14,000 rmp/min at 4°C for 20 mins to obtain supernatant. The supernatant was then dried by speed-vacuum evaporator at 4°C followed by dissolution in 100 μL ice-cold acetonitrile:H_2O (1:1, v/v) for further mass spectrometry analysis. For serum lipid extraction, and comparable to lung samples, 100μL of serum was added to MTBE and methanol (final ratio of MTBE:methanol:serum maintained at 20:6:7 (v/v/v)), sonicated and centrifuged to obtain the upper organic phase. This was followed by drying under nitrogen blow and reconstitution with 50μL isopropanol:-chloroform:methanol (1:1:1, v/v/v) with further dilution with 50 μL initial LC-phases for mass spectrometry analysis. The metabolomics and lipidomics quality control (QC) samples were prepared by mixing identical volumes (as described in the respective figure legends) obtained from all metabolome and/or lipidome samples, respectively.

Instrumental analysis and metabolite-lipid identification

Metabolite and lipid fractions were separated and acquired using an Agilent ultra-high-performance liquid chromatography (1290 UHPLC series, Agilent Technologies, USA) system coupled with quadrupole time-of-flight (Q-TOF) mass spectrometry (6550 iFunnel Q-TOF, Agilent Technologies, USA). Metabolite separation was performed on an Amide column (UPLC BEH Amide,

1.7 μm, 100×2.1 mm, Waters Corporation, Milford, USA) and a hydrophilic interaction chromatography (HILIC) aminopropyl column (3 μm, 150×10 mm, Phenomenex, Torrance, USA) in positive and negative ion mode, respectively. In positive ion mode, the mobile phases comprised of phase A (25 mM NH_4OH and 25 mM NH_4OAc in water) and phase B (ACN), gradient eluted by 95% B (0∼0.5 min); 95% B to 65% B (0.5∼7 min); 65% B to 40% B (7∼8 min); 40% B (8∼9 min); 40% B to 95% (9∼9.1 min) and 95% (9.1∼12 min), with a consistent flow rate of 0.5 mL min^{-1}.Injection volume and column temperature was set at 5 μL and 25°C, respectively. In the negative ion mode, the mobile phases comprised of phase A (ACN: water (5:95, v/v, with 40 mM ammonium hydroxide, pH 9.8)) and phase B (ACN: water (95:5, v/v, with 20 mM ammonium acetate)), gradient eluted by 100% B (0∼2 min); 100% B to 10% B (2∼15 min); 10% B to 0% B (15∼17 min); and 0% B (17∼33 min), with a consistent flow rate of 0.25 mL min^{-1}. Injection volume and column temperature was set at 6μL and 37°C, respectively. Lipid separation was conducted on a C18 Column (UPLC BEH C18, 1.7 μm, 50×2.1 mm, Waters Corporation, Milford, USA) in dual ion modes. The gradient elution comprised of phase A (ACN: water (6:4, v/v, with 10 mM ammonium formate)) and phase B (IPA: ACN (9:1, v/v, with 10 mM ammonium formate)), gradient eluted by 40% to 100% B (0∼10min), 100% B (10∼12min), 100% to 40% B (12∼12.2 min) and 40% B (12.2∼15 min) at a consistent flow rate of 0.4mL min^{-1}. Injection volume and column temperature was set at 5μL and 55°C, respectively. Before running samples for metabolomic and lipidomic analysis, eight QC samples were first run to stabilize the system and then repeated after every six samples to monitor system stability. The acquired raw data was imported into XCMS (Smith et al., 2006) to obtain the ion correction and alignment and significant ions (with *p*-value<=0.05 and |fold change|>=1.5) were selected for further processing. Metabolite and lipid identification was confirmed with reference to the online databases METLIN (Domingo-Almenara et al., 2019), MS-DIAL (Tsugawa et al., 2015) and LipidMaps (Sud et al., 2007).

QUANTIFICATION AND STATISTICAL ANALYSIS

Statistical analysis and data visualization

The Shapiro-Wilk normality test was used to examine data distributions. For continuous variables, statistical significance was determined using Mann-Whitney and/or Kruskal-Wallis test with Dunn's test for post-hoc analysis and Benjimini-Hochberg correction where more than two groups were present. Correlations were assessed using the "rcorr" function within the R package "Hmisc". (Harrell, 2019) For categorial variables, Pearson's Chi-squared test or Fisher's Exact test (as appropriate) was implemented with Bonferroni correction for multiple comparisons when contingency extended beyond 2x2 (MacDonald and Gardner, 2000). In all cases, two-tailed analysis was considered, and differences were deemed significant at $p<0.05$. Analysis was performed using R Statistical Software (v3.5.1) using the "ggplot2" package for visualisation (Wickham, 2016). For microbiome analysis, alpha and beta diversity were assessed using the "vegan" package (Oksanen et al., 2013) while discriminant taxa were identified using by Linear Discriminant Analysis Effect Size (LEfSe, http://huttenhower.sph.harvard.edu/galaxy/) (Segata et al., 2011). Metagenomic data were visualised using MEGAN (Huson et al., 2016).

Transcriptomic analysis, functional enrichment analysis and weighted correlation network analysis

Differential gene expression between treatment groups was analyzed with DESeq2 (Love et al., 2014). Genes were considered differentially expressed when a $\log_2$ Fold Change > ± 1 and false discovery rate < 0.05 was obtained. The functional enrichment analysis of the differentially expressed genes (DEGs) and differential metabolites was performed using Ingenuity Pathway Analysis (IPA) (Qiagen Inc., Germany). The functional network of DEGs and differential metabolites was constructed using Cytoscape (Reimand et al., 2019). Weighted correlation network analysis (WGCNA) was performed to identify gene modules that strongly correlate to temporal changes of serum metabolite markers (Langfelder and Horvath, 2008).